Fermi National Accelerator Laboratory

FERMILAB-Pub-86/100-A
June 1986

NEUTRINO EMISSION BY THE PAIR, PLASMA, AND PHOTO PROCESSES IN THE WEINBERG-SALAM MODEL

Paul J. Schinder[1] and David N. Schramm[1,2]

[1]Department of Astronomy and Astrophysics
University of Chicago, Chicago, Illinois

[2]NASA/Fermilab Astrophysics Center
Fermi National Accelerator Laboratory
Batavia, Illinois

Paul J. Wiita

Department of Astronomy and Astrophysics
University of Pennsylvania, Philadelphia, Pennsylvania

Steven H. Margolis

The Aerospace Corporation
Los Angeles, California

and

David L. Tubbs

Los Alamos National Laboratory
Los Alamos, New Mexico

Operated by Universities Research Association Inc. under contract with the United States Department of Energy

ABSTRACT

The results of numerical integrations of the rates and emissivities of the photo, pair, and plasma neutrino emission mechanisms in the Weinberg-Salam theory of the weak interaction are presented. We consider the range of densities 10 gm $cm^{-3} \leq \rho < 10^{14}$ gm cm^{-3} and the temperature range $10^8 K \leq T \leq 10^{11} K$. We present fitting formulae, similar to those provided by Beaudet, Petrosian, and Salpeter (1967), which reproduce our numerical result for the total emissivity to within 20% in the temperature range $10^{8.2} K \leq T \leq 10^{11} K$.

Subject headings: dense matter – elementary particles – neutrinos

I. INTRODUCTION

Energy loss by neutrino emission is an important process in a wide range of astrophysical problems (Barkat 1975; Tayler 1981). Because neutrinos interact so weakly with matter (typical interaction cross sections are $\approx 10^{-44}\mathrm{cm}^2$ as opposed to typical photon interaction cross sections of $\approx 10^{-24}\mathrm{cm}^2$) they can escape unhindered in circumstances where photons are trapped. Neutrino losses are important in the red giant stages of stellar evolution (*e.g.*, Ramadurai 1976, 1984; Sweigart and Gross 1978), for cooling of white dwarfs (Lamb and Van Horn 1975; Isern *et. al.* 1983) and neutron stars (*e.g.*, Nomoto and Tsuruta 1981), for x-ray burster models (Joss and Li 1980), as well as during supernova collapse (*e.g.*, Bodenheimer and Woosley 1983; Ray, Chitre and Kar 1984).

Beaudet, Petrosian, and Salpeter (1967,hereafter BPS) have presented the results of a series of numerical Monte Carlo integrations of the emission rates of electron neutrinos and antineutrinos due to the pair, photo, and plasma neutrino emission mechanisms (Figure 1) using the "universal" Fermi theory of the weak interaction for a wide range of temperatures and densities. Dicus (1973) rederived the matrix elements for these mechanisms in the Weinberg-Salam theory of the weak interaction, and included the μ neutrino, but did not redo the numerical integrations, instead presenting his results in various limits where analytic approximations may be obtained. Ramadurai (1976,1984) used a modified form of Dicus' correction factors in performing stellar evolutionary calculations, and showed that small, but significant, changes are produced by including these approximations to the effects of neutral currents. The changes in the pair emission rate were also considered by Soyeur and Brown (1979), while modifications to photo neutrino emission rates induced by strong magnetic fields have also been explored (Chou, Fassio-Canuta and Canuto 1979).

In this paper, we present the results of numerical integrations of the pair, photo, and plasma neutrino emission mechanisms in the Weinberg-Salam theory for temperatures between $10^8 K$ and $10^{11} K$ and densities between 10 gm cm^{-3} and 10^{14}gm cm^{-3}. We integrate numerically to find the emissivities (erg cm^{-3} sec^{-1}) and rates (cm^{-3} sec^{-1}) of electron, μ and τ neutrinos. We also, following the example of BPS, present fitting formulae for our emissivities. However, we will show that the BPS fitting formulae must be used with great caution. The individual fitting formulae which they give are very poor fits to our recalculation of the neutrino emissivities in the Fermi theory and are a reasonable fit only to the *total* emissivity, and only in the region in which BPS calculated actual values for the emissivities. The granularity of their grid is evident in their fitting formulae, as we shall show.

Flowers (1972) investigated the role of neutrino-pair bremsstrahlung as a as a cooling mechanism in matter below its melting temperature in the Fermi theory; this was originally considered by Festa and Ruderman (1969). Dicus, Kolb, Schramm, and Tubbs (1976) subsequently included neutral current effects. We do not consider this reaction here, since Flowers shows it is important only at high densities, where it begins to dominate as the plasma neutrino emissivity drops rapidly, and Dicus, Kolb, Schramm, and Tubbs show that including neutral currents does not change the results greatly. Recently Itoh and Kohyama and collaborators (Itho and Kohyama 1983; Itoh, *et. al.* 1984 a,b,c) have improved upon the calculations for neutrino-pair bremmstrahlung by including corrections due to phonons in the crystalline lattice phase and low-temperature quantum corrections to the liquid metal phase. Adding the fitting formulae they present for those reactions to the ones we give below provides a fairly complete description of neutrino emissivities over

a very broad range in temperature and density.

As we were completing this work, we learned of the similar work of Munakata, Kohyama, and Itoh (1985), who presented the neutrino emissivities for the pair, plasma, and photo neutrino processes in the temperature range $10^8 K \leq T \leq 10^{10} K$ and in the density range 1 gm cm$^{-3} \leq \rho \leq 10^{14}$ gm cm^{-3}. Our expressions for the neutrino emissivities given below are identical to theirs, but our photo neutrino emissivity for $T = 10^8 K$ seems to differ appreciably from theirs. However, because it is difficult to read many cycle log-log plots or compare them with each other, the difference may or may not be real. Munakata et al. also present fitting formulae for the three emissivities. We have used their fitting formulae to compare with our results by computing their fitting formulae, using $sin^2\theta_W = 0.23$ instead of the value 0.217 which they use, over the range of temperatures and densities for which we have numerical results. The results of this test show that in general, the simple fitting formulae which we present below are better fits to our numerical data than their more complicated formulae. If their fitting formulae are accurate representations of their numerical results, the discrepancy between our numerical results and theirs at low temperatures ($10^8 - 10^9 K$) may be $> 10\%$ at densities where the photo neutrino process dominates. As might be expected, their fitting formulae are poor (errors $> 40\%$ at $T = 10^{11} K$) in the high temperature regime ($10^{11} K$) which they do not inspect.

In §II, we will present the results of our numerical integrations, going briefly into the techniques. Since there are minor errors in the published literature about the photo neutrino rates, we will more fully discuss the photo neutrino rate, and present the numerical technique used to calculate the integrals for those rates, in the Appendix. In §III, we will present our results and discuss our fitting formulae to our numerical results. We will show

that the fitting formulae provided by BPS are actually poor fits to our recalculations of the Fermi emissivities (which agree well with their data), and only fit the *sum* of the three rates with any degree of accuracy. In §IV, we will summarize our findings.

II. BASIC FORMULA AND NUMERICAL TECHNIQUES

The basic equations for the photo, pair, and plasma neutrino emission mechanisms are given in Dicus(1973). We will present his results below, with the minor modifications necessary to include both μ and τ neutrinos.

The emissivity (erg cm^{-3} sec^{-1}) due to the pair neutrino reaction ($e^+ + e^- \rightarrow \nu_{e,\mu,\tau} + \bar{\nu}_{e,\mu,\tau}$) is given by

$$\begin{aligned} \mathcal{Q}_{pair} = \frac{G_W^2 m^9 c^9}{18\pi^5\hbar^{10}}\{&(7\mathcal{C}_V^2 - 2\mathcal{C}_A^2)[G_0^- G_{-1/2}^+ + G_{-1/2}^- G_0^+] + 9\mathcal{C}_V^2[G_{1/2}^- G_0^+ + G_0^- G_{1/2}^+] \\ &+ (\mathcal{C}_V^2 + \mathcal{C}_A^2)[4G_1^- G_{1/2}^+ + 4G_{1/2}^- G_1^+ - G_1^- G_{-1/2}^+ - G_{1/2}^- G_0^+ - G_0^- G_{1/2}^+ - G_{-1/2}^- G_1^+]\}, \end{aligned} \tag{1}$$

where

$$G_n^{\pm}(\lambda,\nu) \equiv \lambda^{3+2n}\int_{\lambda^{-1}}^{\infty} dx \frac{x^{2n+1}(x^2-\lambda^{-2})}{e^{x\pm\nu}+1}, \tag{2}$$

G_W is the Fermi constant $= 1.435 \times 10^{-49}$erg cm^3, $\mathcal{C}_V^2 = C_V^2 + 2(C_V - 1)^2$, $\mathcal{C}_A^2 = C_A^2 + 2(C_A - 1)^2$, $C_A = 1/2$, $C_V = 1/2 + 2\sin^2\theta_W$, and θ_W is the weak angle. In these calculations we use $\sin^2\theta_W = 0.23$. The rate (cm^{-3} sec^{-1}) due to the pair neutrino reaction is given by

$$\begin{aligned} \mathcal{R}_{pair} = \frac{G_W^2 m^8 c^7}{18\pi^5\hbar^{10}}\{&(7\mathcal{C}_V^2 - 2\mathcal{C}_A^2)[G_{-1/2}^- G_{-1/2}^+] + 9\mathcal{C}_V^2[G_0^- G_0^+] \\ &+ (\mathcal{C}_V^2 + \mathcal{C}_A^2)[4G_{1/2}^- G_{1/2}^+ - G_{1/2}^- G_{-1/2}^+ - G_{-1/2}^- G_{1/2}^+]\}. \end{aligned} \tag{3}$$

The emissivity and the rate due to the plasma neutrino reaction (plasmon $\rightarrow \nu_{e,\nu,\tau} + \bar{\nu}_{e,\nu,\tau}$) may each be split into two parts, that due to longitudinal plasmons (which may be thought of as collective excitations of the electron gas), and that due to transverse

plasmons (normal photons interacting with the electron gas). The longitudinal emissivity is

$$\mathcal{Q}_L = \frac{G_W^2 m^9 c^9}{48\pi^4\hbar^{10}\alpha}\frac{1}{2}\left(\frac{5}{3}\right)^{\frac{7}{2}} C_V^2 \gamma^9 \lambda^9 \left(\frac{\omega_o}{\omega_1}\right)^7 \int_1^a \frac{y^{10}(y^2-a^2)^2\sqrt{y^2-1}}{e^{\gamma y}-1}dy, \qquad (4a)$$

where $a^2 = 1 + (3/5)(\omega_1/\omega_o)^2$ and the transverse emissivity is given by

$$\mathcal{Q}_T = \frac{G_W^2 m^9 c^9}{48\pi_4\hbar^{10}\alpha} C_V^2 \gamma^6 \lambda^9 \int_\gamma^\infty \frac{x\sqrt{x^2-\gamma^2}}{e^x-1}dx, \qquad (4b)$$

where $\gamma = (\hbar\omega_o)/(kT)$, $\lambda = (kT)/(mc^2)$, ω_o is the plasma frequency given by

$$\omega_o^2 = \frac{4\alpha(mc^2)^2}{3\pi\hbar^2}[2G^+_{-1/2} + 2G^-_{-1/2} + G^+_{-3/2} + G^-_{-3/2}],$$

ω_1 is the first order correction to the plasma frequency given by

$$\omega_1^2 = \omega_o^2 - \frac{4\alpha(mc^2)^2}{3\pi\hbar^2}[3G^+_{-5/2} + 3G^-_{-5/2}],$$

m is the mass of the electron, and α is the fine structure constant. Note that this differs from the results of BPS only by a factor of $C_V^2 = 0.928$, and is not valid at low density and high temperature as they explain. The longitudinal rate is given by

$$\mathcal{R}_L = \frac{G_W^2 m^8 c^7}{48\pi_4\hbar^{10}\alpha}\frac{1}{2}\left(\frac{5}{3}\right)^{\frac{7}{2}} C_V^2 \gamma^8 \lambda^8 \left(\frac{\omega_o}{\omega_1}\right)^7 \int_1^a \frac{y^9(y^2-a^2)\sqrt{y^2-1}}{e^{\gamma y}-1}dy, \qquad (5a)$$

and the transverse rate is

$$\mathcal{R}_T = \frac{G_W^2 m^8 c^7}{48\pi_4\hbar^{10}\alpha} C_V^2 \gamma^6 \lambda^8 \int_\gamma^\infty \frac{\sqrt{x^2-\gamma^2}}{e^x-1}dx, \qquad (5b)$$

The emissivity for the photo neutrino reaction ($e^\pm + \gamma \rightarrow e^\pm + \nu_{e,\nu,\tau} + \bar{\nu}_{e,\nu,\tau}$) is more complicated than the previous two reactions:

$$\mathcal{Q}_{photo} = \frac{(kT)^5}{4(2\pi)^7}\int_{\lambda^{-1}}^\infty dx\,\sqrt{x^2-\lambda^{-2}}\,(e^{x-\nu}+1)^{-1}\int_\gamma^\infty dy\,\sqrt{y^2-\gamma^2}\,(e^y-1)^{-1}\int_{-1}^1 dw$$
$$\times\int_0^1 \frac{t^2\,dt\,m^2}{SD(D+2)}\int_{-1}^1 dz\,(x+y)\left(1-\frac{S+Gtz}{D+2}\right) I(e^{\nu-\frac{S-Gtz}{D-2}(-x-y)}+1)^{-1} \qquad (6),$$

where the various terms are defined in equation (A12) of the Appendix. The corresponding rate is found by simply removing the factor of $(x+y)$ from the integrand in equation 6 and removing one power of kT from the coefficient in front of the integral. Note that, where the plasma and pair emissivities and rates can be written in terms of (relatively) simple one dimensional integrals, the photo production emissivity (and the corresponding rate) is a five dimensional integral and must be done by a Monte Carlo technique.

We use a standard numerical technique, the Romberg method (Acton 1970), to integrate the plasma and pair emissivities and rates. Four significant figures are required from the integration routine, and in most cases are obtained. Only for low temperatures and high densities does the integration routine fail to provide four figures; in those cases, three significant figures are found. Results calculated with $C_V = C_A = 1$ reproduce very well the results obtained by BPS. The photo neutrino emissivity and rate are done by a Monte Carlo integration routine, more fully described in the Appendix. The formal errors in the integration are a few percent. Setting $C_V = C_A = 1$ reproduces the BPS results very accurately.

III. NUMERICAL RESULTS AND FITTING FORMULAE

Figure 2 shows our results for the emissivities for $T = 10^8 K$, $T = 10^9 K$, $T = 10^{10} K$, and $T = 10^{11} K$ for densities in the range 10 gm cm^{-3} $< \rho <$ 10^{14}gm cm^{-3}. Figure 3 shows our results for the rates for the same four temperatures in the same density range. The photo neutrino process is important only in the temperature range $10^8 K \leq T \lesssim 10^9 K$. The pair neutrino process dominates the low density regime for temperature above $10^9 K$, while the plasma process dominates at high density for all temperatures considered here.

Figure 3 shows the average energy of the emitted neutrinos and antineutrinos, $E_{av} \equiv$

$\mathcal{Q}/\mathcal{R}$, in units of keV. Notice that the pair neutrino process emits the most energetic neutrinos and antineutrinos for all T. The average energy of pair neutrinos at $T = 10^8 K$ is not shown since the pair emissivity is completely negligible compared to the photo and pair emissivities there.

Note that the photo neutrino results do not extend beyond $\rho \gtrsim 10^{11}$ gm cm^{-3}. This is because the plasma frequency ω_o becomes $> 2m_e c^2/\hbar$. At this point, numerical difficulties prevent further calculation. However, by this time the plasma neutrino process is so enormously dominant that we felt no need to continue calculations of the photo neutrino emissivity and rate. BPS show that the photo neutrino emissivity at high density is $\sim 10^{-6}$ of the plasma neutrino emissivity. The reaction plasmon $\rightarrow e^+ + e^- + \nu + \bar{\nu}$ can also occur when the plasma frequency exceeds $2m_e c^2/\hbar$.

The photoneutrino results shown in figures 2, 3, and 4 were done using 50000 random points for the Monte Carlo integration. The formal errors are less than a percent for all densities and temperatures where the photoneutrino emissivity dominates. The formal error increased rapidly at high densities where the electron degeneracy becomes large. We also performed Monte Carlo calculations using a finer grid in $\rho - T$ space using only 5000 random points for each integration. The temperature range covered was from $10^8 K \leq T \leq 10^{11} K$ in steps of $\Delta \log(T(K)) = 0.1$ and the density range was 10^1 gm cm$^{-3} \leq \rho \leq 10^{14}$ gm cm^{-3} in steps of $\Delta \log([\rho/\mu_e](\text{gm cm}^{-3})) = 0.125$. The formal errors were only a few percent for those densities and temperatures where the photoneutrino emissivity dominates. The 5000 point results agree very well with the more accurate 50000 point results for those temperatures and densities where they were both calculated. The 5000 point results were used to calibrate our fitting formulae, which we now present.

BPS calculated the emissivities for the three processes at 260 points in $\rho - T$ space. They sampled density in steps of $10^{0.5}$ gm cm^{-3} between 1 gm cm^{-3} and 10^{14} gm cm^{-3}, and temperature in steps of $10^{0.2}K$ between 10^8K and $10^{10}K$. They fit their results to

$$Q_{approx} = K(\rho,\lambda)e^{-c\xi}\left(\frac{a_0 + a_1\xi + a_2\xi^2}{\xi^3 + b_1/\lambda + b_2/\lambda^2 + b_3/\lambda^3}\right), \tag{7a}$$

where $\lambda = T/5.9302 \times 10^9K$,

$$\xi = \left(\frac{\rho/\mu_e}{10^9 \text{ gm cm}^{-3}}\right)^{\frac{1}{3}}\lambda^{-1}, \tag{7b}$$

$$K(\rho,\lambda) = \begin{cases} (\rho/\mu_e)^3 & \text{plasma} \\ (\rho/\mu_e)\lambda^5 & \text{photo} \\ g(\lambda)e^{-(2/\lambda)} & \text{pair} \end{cases}, \tag{7c}$$

$g(\lambda) = 1 - 13.04\lambda^2 + 133.5\lambda^4 + 1534\lambda^6 + 918.6\lambda^8$ and a_0, a_1, a_2, b_1, b_2, b_3, and c are adjustable parameters. BPS give values for these parameters in Table 2 of their paper. Because we have actual numerical results on a finer grid, the BPS fitting formula can be tested for points in $\rho - T$ space for which they did not calculate emissivities. Figure 5 shows a comparison of the BPS fitting formula with our recalculation of the emissivities in the Fermi theory for two temperatures: $T = 10^8K$, which is a point at which BPS did calculate the emissivities, and $T = 10^{8.1}K = 1.259 \times 10^8K$. Notice that the fit is quite good at $T = 10^8K$, deviating significantly only at high densities when the plasma neutrino emissivity is dropping steeply as a function of ρ/μ_e. However, the result is completely different at $T = 10^{8.1}K$; notice that the error is as much as 70%. The maximum error occurs at about $\rho/\mu_e \approx 10^5$ gm cm^{-3}, where the plasma neutrino emissivity dominates, so the error is not due to possible errors in our Monte Carlo integrations. This is the worst case that we found in the temperature interval $10^8K \leq T \leq 10^{10}K$, but it indicates that the BPS fitting formulae must be used with extreme caution, paying full heed to the

warnings contained in that work. In the interval $10^{10} \leq T \leq 10^{11}$, we find that the error in the fitting formula increases to about 40% at $T = 10^{11} K$ (figure 6).

Dicus (1973) provided approximate multiplicative factors by which to multiply the BPS fitting formulae to convert to the Weinberg-Salam theory of the weak interaction. We choose from Dicus the following multiplicative factors to construct the fits we present below: the plasma neutrino emissivity is multiplied by a factor of $C_V^2 + 2(C_V - 1)^2 = 0.925$, the pair neutrino emissivity is multiplied by the same factor, and the photo neutrino emissivity is multiplied by a factor of $(C_V^2 + 2(C_V - 1)^2 + 5C_A^2 + 10(C_A - 1)^2)/6 = 0.7791$. We checked these coefficients by comparing Dicus' predictions with the results we actually obtain by numerical integration. Figure 7 shows the quantity $\Delta Q/Q$, where $\Delta Q \equiv (Q - Q_{approx})$, *vs.* ρ/μ_e for three values of temperature: $T = 10^8 K$, $T = 10^9 K$, and $T = 10^{10} K$. As can be seen in the figure, the fits are reasonably good except at high density, where the plasma neutrino rate is falling sharply. Table 1 presents the numerical values of the coefficients which we use. The maximum error which we find in the temperature range $10^{8.2} K \leq T \leq 10^{10} K$ is about 20%. The error at $10^{8.1} K$ has a maximum of ~60%.

In the interval $10^{10} K < T \leq 10^{11} K$, we modified the coefficients in the BPS fitting formula by hand to construct a fitting formula which more nearly fits our results in this region. The coefficients we use are also given in Table 1. Figure 8 compares this fitting formula with our numerical results for $T = 10^{10.5} K$ and $T = 10^{11} K$. The most difficult regions to fit are those where the pair and plasma neutrino emissivities begin to drop rapidly.

IV. CONCLUSION

In this paper, we have presented the results of our numerical calculations of the photo,

pair, and plasma neutrino emissivities and rates of matter in the Weinberg-Salam theory of the weak interaction. We also compared our recalculation of the photo, pair, and plasma neutrino emissivities in the "universal" Fermi theory of the weak interactions with the fitting formulae given by BPS. We find that the BPS fitting formula are good fits to our recalculations only in the interval of temperature in which they calculated actual values of the emissivities ($10^8 K \leq T \leq 10^{10}$), and can be significantly in error near the edges of this region (we find 70% differences between the BPS fitting formula and our numerical results at $T = 10^{8.1} K$). We show that the multiplicative factors provided by Dicus (1973) to convert the BPS formulae to the Weinberg-Salam theory are good, and the fitting formulae using these correction factors agree reasonably well with our Weinberg-Salam theory results in the temperature region $10^{8.2} K \leq T \leq 10^{10} K$. We provide additional fitting formula which fit the region $10^{10} K < T \leq 10^{11} K$ reasonably well ($\approx$ 20% maximum error).

ACKNOWLEDGEMENTS

This work was supported by NSF grant AST83-13128 at the University of Chicago, and by NSF grant AST82-11065 at the University of Pennsylvania. PJS would like to thank the Computer Science Department of the University of Chicago for the use of their computers, and DOE/Fermilab for access to the MFE computing facility at Lawrence Livermore.

APPENDIX

In this appendix, we will derive in detail the photoneutrino emissivity due to $e^{\pm} + \gamma \rightarrow e^{\pm} + \nu_e + \bar{\nu}_e$. The derivation for the emissivity in the Fermi theory of the weak interaction is given in Beaudet, Petrosian and Salpeter (1967) while the derivation in the Weinberg-Salam theory is given in Dicus (1973). There are small errors in both, which we attempt to correct here. We use units $\hbar = c = 1$, and Dirac spinors are normalized to $\bar{u}u = 2E$. Otherwise, we use the conventions of Bjorken and Drell(1964). To obtain the emissivity for $e^{\pm} + \gamma \rightarrow e^{\pm} + \nu_{\mu,\tau} + \bar{\nu}_{\mu,\tau}$, simply do the usual replacement $C_V \rightarrow C_V - 1$, $C_A \rightarrow C_A - 1$ in what appears below. The total emissivity of all three neutrino types is obtained by replacing $C_V^2 \rightarrow C_V^2 + 2(C_V - 1)^2$, $C_A^2 \rightarrow C_A^2 + 2(C_A - 1)^2$ in what appears below.

The emissivity is given by

$$\mathcal{Q} = \int \frac{d^3p}{(2\pi)^3} 2 f_e(E) \int \frac{d^3k}{(2\pi)^3} 2 f_\gamma(\omega) \int \frac{d^3p'}{(2\pi)^3} (1 - f_e(E')) \int \frac{d^3q}{(2\pi)^3} \int \frac{d^3q'}{(2\pi)^3} \times (2\pi)^4 \delta^4(p + k - p' - q - q')(E + \omega - E') \left(\frac{1}{4}\right) \sum_{s,\epsilon} |M|^2 \left\{ \frac{1}{2E} \frac{1}{2E'} \frac{1}{2\omega} \frac{1}{2q_0} \frac{1}{2q_0'} \right\} \quad (A1),$$

where $p = (E, \mathbf{p})$ is the four momentum of the incoming electron, $p' = (E', \mathbf{p}')$ is the four momentum of the final electron, $k = (\omega, \mathbf{k})$ is the four momentum of the incoming photon, $q = (q_0, \mathbf{q})$ is the four momentum of the emitted neutrino, and $q' = (q_0', \mathbf{q}')$ is the four momentum of the emitted antineutrino. The corresponding rate is found by simply removing the expression $E + \omega - E'$ from equation (A1). In equation (A1), $f_e(E) = (exp((E - \mu)/kT) + 1)^{-1}$ is the electron distribution function, where μ is the electron chemical potential, and $f_\gamma(\omega) = (exp(\omega/kT) - 1)^{-1}$ is the photon distribution function. The factor of 2 in front of $f_e(E)$ and $f_\gamma(\omega)$ take into account the two spin states of those particles, while the factor of 1/4 preceding the sum averages over initial spin states. In the sum, the index s indicates sums over electron spin states (both initial and final), while

ϵ indicates a sum over the initial photon spin states.

Continuing, three angular integrals may be done immediately, yielding

$$\begin{aligned}\mathcal{Q} =&\frac{2(2\pi)^2}{8(2\pi)^9}\int_0^\infty \frac{p^2dp}{E}f_e(E)\int_0^\infty \frac{k^2dk}{\omega}f_\gamma(\omega)\int_{-1}^1 dw\int \frac{d^3p'}{E'}(1-f_e(E'))\\ &\times\int\frac{d^3q}{2q_0}\int\frac{d^3q'}{2q_0'}\frac{1}{(2\pi)^2}\delta^4(p+k-p'-q'-q)(E+\omega-E')\sum_{s,\epsilon}|M|^2\end{aligned} \qquad (A2),$$

where $w=\cos(\mathbf{p},\mathbf{k})$.

We now define, following Dicus equation (39),

$$I=\int\frac{d^3q}{2q_0}\int\frac{d^3q'}{2q_0'}\frac{1}{(2\pi)^2}\delta^4(p+k-p'-q-q')\sum_{s,\epsilon}|M|^2 \qquad (A3),$$

so that

$$\mathcal{Q}=\frac{1}{4(2\pi)^7}\int_0^\infty\frac{p^2dp}{E}f_e(E)\int_0^\infty\frac{k^2dk}{\omega}f_\gamma(\omega)\int\frac{d^3p'}{E'}(1-f_e(E'))(E+\omega-E')I \qquad (A4).$$

Equation (A4) agrees with BPS equation (B3), and differs by a factor of 1/4 with Dicus equation (40).

We now find $\sum_s|M|^2$. The matrix element M is given by Dicus

$$\begin{aligned}M=&-\frac{ieg^2}{8m_W^2}\bar{u}_e(p')\gamma^\alpha(C_V-C_A\gamma_5)\frac{\not p'+\not k+m}{2p'\cdot k+\omega_o^2}\not\epsilon u_e(p)\bar{u}_\nu(q)\gamma_\alpha(1-\gamma_5)v_\nu(q')\\ &-\frac{ieg^2}{8m_W^2}\bar{u}_e(p')\frac{\not p'-\not k+m}{-2p'\cdot k+\omega_o^2}\gamma^\alpha(C_V-C_A\gamma_5)u_e(p)\bar{u}_\nu(q)\gamma_\alpha(1-\gamma_5)v_\nu(q')\end{aligned} \qquad (A5),$$

where ω_o is the plasma frequency. The quantity $\sum_s|M|^2$ is

$$\begin{aligned}\sum_s|M|^2=&\frac{e^2g^4}{64m_W^4}Tr\Big[(\not p'+m)\{\gamma^\alpha(C_V-C_A\gamma_5)\frac{\not Q_1+m}{\beta_1}\not\epsilon+\not\epsilon\frac{\not Q_2+m}{\beta_2}\gamma^\alpha(C_V-C_A\gamma_5)\}(\not p+m)\\ &\times\{(C_V+C_A\gamma_5)\gamma^\beta\frac{\not Q_2+m}{\beta_2}\not\epsilon+\not\epsilon\frac{\not Q_1+m}{\beta_1}(C_V+C_A\gamma_5)\gamma^\beta\}\Big]\\ &\times Tr\Big[\not q\gamma_\alpha(1-\gamma_5)(-\not q')(1+\gamma_5)\gamma_\beta\Big]\end{aligned} \qquad (A6),$$

where $Q_1=p+k$, $Q_2=p'-k$, $\beta_1=(p+k)^2-m^2=2k\cdot p+\omega_o^2$, $\beta_2=(p'-k)^2-m^2=-2p'\cdot k+\omega_o^2$, and m is the mass of the electron. We use Leanard's formula

$$\int\frac{d^3q}{2q_0}\int\frac{d^3q'}{2q_0'}\delta^4(P-q-q')q^\mu q'^\nu=\frac{\pi}{24}\Theta(P^2)(2P^\mu P^\nu+g^{\mu\nu}P^2),$$

where

$$\Theta(P^2) = \begin{cases} 1 & \text{if } P^2 \geq 0; \\ 0 & \text{if } P^2 < 0, \end{cases}$$

to integrate over d^3q and d^3q', and taking the second trace, find

$$\begin{aligned} I =& \Theta(P^2)\frac{1}{96\pi}(32P_\alpha P_\beta - 32g_{\alpha\beta}P^2)\sum_\epsilon \frac{e^2g^4}{64m_W^4} Tr\Big[(\not{p}' + m)\{\gamma^\alpha(C_V - C_A\gamma_5)\frac{\not{Q}_1 + m}{\beta_1}\not{\epsilon} \\ &+ \not{\epsilon}\frac{\not{Q}_2 + m}{\beta_2}\gamma^\alpha(C_V - C_A\gamma_5)\}(\not{p} + m)\{(C_V + C_A\gamma_5)\gamma^\beta\frac{\not{Q}_2 + m}{\beta_2}\not{\epsilon} \\ &+ \not{\epsilon}\frac{\not{Q}_1 + m}{\beta_1}(C_V + C_A\gamma_5)\gamma^\beta\}\Big] \end{aligned} \tag{A7}$$

where $P = p + k - p'$. We will split I into two parts, $I_+ \propto (C_V^2 + C_A^2)$, and $I_- \propto (C_V^2 - C_A^2)$. Making use of the facts that $\epsilon \cdot \epsilon = -1$, $\epsilon \cdot p = 0$ (by choice; see below), and $\epsilon \cdot k = 0$, after performing the remaining trace, we find, using $G^2 = g^4/(32m_W^4)$,

$$\begin{aligned} I_- =& \Theta(P^2)\frac{e^2G^2}{6\pi}(C_V^2 - C_A^2)m^2\sum_\epsilon\Big[\frac{12P^2}{\beta_2^2}\omega_o^2 + \frac{12P^2}{\beta_1^2}\omega_o^2 - \frac{8}{\beta_1\beta_2}(P^2\omega_o^2 - 2(k\cdot P)^2) \\ &-(p'\cdot\epsilon)^2\left\{\frac{16\omega_o^2}{\beta_1\beta_2} + \frac{48P^2}{\beta_2^2}\right\}\Big] \end{aligned} \tag{A8a}$$

$$\begin{aligned} I_+ =& \Theta(P^2)\frac{G^2e^2}{3\pi}(C_V^2 + C_A^2)\sum_\epsilon\Big\{4P^2 + P^2(P^2 - m^2)\Big[2\omega_o^2\left(\frac{1}{\beta_1} + \frac{1}{\beta_2}\right)^2 - \frac{8}{\beta_2^2}(\epsilon\cdot p')^2\Big] \\ &- \frac{8}{\beta_1\beta_2}(P^2 + m^2)(k\cdot P)^2 - \frac{8}{\beta_1\beta_2}\omega_o^2P^2\left[P^2 - 2m^2 - (k\cdot P) + \frac{\omega_o^2}{2}\right] \\ &+ \frac{8}{\beta_1\beta_2}\omega_o^2(P^2 + m^2)(\epsilon\cdot p')^2\Big\} \end{aligned} \tag{A8b}$$

We now perform the sum over photon polarization states. Following BPS, we choose $\epsilon^\mu = (0, \varepsilon)$ in the rest frame of the initial electron. Then, in this frame

$$(\epsilon\cdot p) = 0,$$

$$\sum_\epsilon(\epsilon\cdot p')^2 = |\mathbf{p}'|^2 - \frac{(\mathbf{p}'\cdot\mathbf{k})^2}{|\mathbf{k}|^2}.$$

The first equation is true in all frames. We write the second in terms of relativistic

invariants, with $u = p/m$ the four velocity of the initial electron,

$$\sum_{\epsilon}(p'\cdot\epsilon)^2 = (p'\cdot u)^2 - p'^2 - \frac{((p'\cdot u)(k\cdot u) - p'\cdot k)^2}{((k\cdot u)^2 - k^2)}.$$

So, in any frame

$$\begin{aligned}\sum_{\epsilon}(p'\cdot\epsilon)^2 = \left(\frac{-1}{(k\cdot p)^2 - m^2\omega_o^2}\right)\Big[&\frac{1}{2}(2p\cdot k + \omega_o^2)(2p'\cdot k - \omega_o^2)(m^2 - p\cdot p') \\ &+m^2(k\cdot(p+k-p'))^2 - \frac{1}{2}\omega_o^2(m^2 + p\cdot p')(p+k-p')^2\Big]\end{aligned} \tag{A9}$$

After doing the summation, $I = I_+ + I_-$ becomes, with $\beta^{-1} \equiv \beta_1/2$ and $\gamma^{-1} \equiv -\beta_2/2$ to conform with the notation used by Dicus and BPS, and inserting the factor of 2 due to the sum over photon polarizations of terms not prorportional to $\sum_\epsilon(p'\cdot\epsilon)^2$,

$$\begin{aligned}I_- =&\Theta(P^2)\frac{e^2G^2}{6\pi}(C_V^2 - C_A^2)m^2\Big[6P^2\beta^2\omega_o^2 + 6P^2\gamma^2\omega_o^2 + 4\beta\gamma(P^2\omega_o^2 - 2(k\cdot P)^2) \\ &+ (-4\omega_o^2\beta\gamma + 12P^2\gamma^2)\left(\frac{1}{(k\cdot p)^2 - m^2\omega_o^2}\right)\Big\{2(\beta\gamma)^{-1}(m^2 - p'\cdot p) \\ &+ m^2(k\cdot P)^2 - \frac{1}{2}\omega_o^2(m^2 + p\cdot p')P^2\Big\}\Big]\end{aligned} \tag{A10a}$$

$$\begin{aligned}I_+ =&\Theta(P^2)\frac{2G^2e^2}{3\pi}(C_V^2 + C_A^2)\Big\{4P^2 + 2\beta\gamma(P^2 + m^2)(k\cdot P)^2 + 2\beta\gamma\omega_o^2P^2 \\ &\times\left[P^2 - 2m^2 - (k\cdot P) + \frac{\omega_o^2}{2}\right] + \frac{\omega_o^2}{2}(\beta-\gamma)^2P^2(P^2 - m^2) \\ &+ [\gamma^2P^2(P^2 - m^2) + \beta\gamma\omega_o^2(P^2 + m^2)] \\ &\times\left(\frac{1}{(k\cdot p)^2 - m^2\omega_o^2}\right)\Big\{2(\beta\gamma)^{-1}(m^2 - p'\cdot p) \\ &+ m^2(k\cdot P)^2 - \frac{1}{2}\omega_o^2(m^2 + p\cdot p')P^2\Big\}\Big\}\end{aligned} \tag{A10b}$$

Now we will get equation (A4) into a form suitable for Monte Carlo integration. We will follow the treatment of BPS closely. Because of the factor $\Theta(P^2)$, the most convenient frame to do the $\int d^3p'$ is in the center of momentum of the initial particles, where the constraint becomes $\Theta((2p\cdot k + \omega_o^2)/(2|p+k|) - |\mathbf{p}'_{\mathbf{CM}}|)$. Defining

$$\omega' = \frac{2p\cdot k + \omega_o^2}{2|p+k|},$$

$\mathcal{Q}$ becomes

$$\begin{aligned}\mathcal{Q} =& \frac{1}{4(2\pi)^7}\int_0^\infty \frac{p^2dp}{E} f_e(E)\int_0^\infty \frac{k^2dk}{\omega} f_\gamma(\omega)\int_0^{\omega'} p'^2_{CM}dp'_{CM} \\ & \times \int_{-1}^{1} dz \int_0^{2\pi} d\phi_{CM}(1-f_e(E'))(E+\omega-E')I\end{aligned} \qquad (A11),$$

where the z axis is aligned along the direction of $\mathbf{p}+\mathbf{k}$ so that $z = \cos(\mathbf{p}+\mathbf{k}, \mathbf{p'}_{CM})$. We align the x axis in the direction of $\mathbf{p}+\mathbf{k}-\mathbf{k}_{CM}$, and define $\Lambda = \cos(\mathbf{p}+\mathbf{k}, \mathbf{k}_{CM})$, $\alpha = \cos(\mathbf{k}_{CM}, \mathbf{p'}_{CM})$ so that $\alpha = z\Lambda + \sqrt{1-z^2}\sqrt{1-\Lambda^2}\cos\phi_{CM}$. The integral over ϕ_{CM} may then be performed, and the result is

$$\begin{aligned}\mathcal{Q} =& \frac{(kT)^5}{4(2\pi)^7}\int_{\lambda^{-1}}^\infty dx\sqrt{x^2-\lambda^{-2}}\,(e^{x-\nu}+1)^{-1}\int_\gamma^\infty dy\sqrt{y^2-\gamma^2}\,(e^y-1)^{-1}\int_{-1}^1 dw \\ & \times\int_0^1 \frac{t^2\,dt\,m^2}{SD(D+2)}\int_{-1}^1 dz\,(x+y)\left(1-\frac{S+Gtz}{D+2}\right)I(e^{\nu-\frac{S+Gtz}{D+2}(x+y)}+1)^{-1}\end{aligned} \qquad (A12),$$

where $x = E/kT$, $y = \omega/kT$, $\lambda = kT/m$, $\gamma = \omega_o/kT$, $t = p'_{CM}/\omega'$, $\nu = \mu/kT$,

$$\begin{aligned}I =& I_+ + I_-, \\ I_+ =& \frac{16G^2m^2e^2}{3}(C_V^2+C_A^2)\left(\frac{1}{D}\right)\Big\{(1+D-S)\Big[2+C(1+LF^{-\frac{1}{2}}(2+C-4S))\Big] \\ & +(1+D-S)(1+\frac{1}{2}D-S)\Big[\frac{C}{2}\Big(1-4LF^{-\frac{1}{2}}+4L^2F^{-\frac{3}{2}}(U-tBz)\Big) \\ & +EL\Big(1-2UF^{-\frac{1}{2}}+VF^{-\frac{3}{2}}(U-tBz)\Big)\Big] \\ & +(1+\frac{3}{2}D-S)\left[2LF^{-\frac{1}{2}}-2+\frac{U-tBz}{2L}+\frac{EC}{4}\Big(-2U+(U-tBz)+VF^{-\frac{1}{2}}\Big)\right]\Big\}, \\ I_- =& \frac{1}{4}\frac{16G^2m^2e^2}{3}(C_V^2-C_A^2)\Big\{C(1+D-S)\Big(3+4LF^{-\frac{1}{2}}+12F^{-\frac{3}{2}}L^2(U-tBz)\Big) \\ & -4LF^{-\frac{1}{2}}+4-\frac{U-tBz}{L}+6EL(1+D-S)\Big[1-2UF^{-\frac{1}{2}}+(U-tBz)VF^{-\frac{3}{2}}\Big] \\ & -\frac{CE}{2}\Big[(U-tBz)-2U+VF^{-\frac{1}{2}}\Big]\Big\}\end{aligned}$$

$$D = \frac{2m^2}{2p\cdot k + \omega_o^2},$$
$$C = \frac{\omega_o^2}{m^2} D,$$
$$S = \sqrt{D(D+2) + t^2},$$
$$L = \frac{D+2}{C+2},$$
$$U = S - LC,$$
$$E = \frac{4}{C + 2 - 4LC},$$
$$G = \sqrt{1 - \frac{D+2}{\lambda^2 (x+y)^2 D}},$$
$$B = \frac{2Ly - x - y}{G(x+y)},$$
$$K = \frac{2}{\sqrt{(2+C)E}},$$
$$V = \frac{2L}{2+C}[2D - C(1+D-S)(2D+2S-C)],$$
$$F = (U - tBz)^2 - (1-z^2)(K^2 - B^2)t^2.$$

This expression for I is valid for $(U - tBz)^2 > (1-z^2)(K^2 - B^2)t^2$. If $(U - tBz)^2 \leq (1-z^2)(K^2 - B^2)t^2$, a non-integrable singularity appears in the integral over ϕ_{CM}. We find that this occurs only when $\omega_o > 2m$, at densities $\rho \gtrsim 10^{11}$ gm cm^{-3}. When $\omega_o > 2m$, the photon can also decay via the mode $\gamma \rightarrow e^+ + e^-$. The dielectric constant (and hence the plasma frequency) becomes complex, and a more exact treatment of the physics is needed. We have not investigated this further, since the densities at which $\omega_o > 2m$ lie at the extreme upper end of the range of interest, where the plasma neutrino emissivity always dominates the photo neutrino emmisivity by orders of magnitude. The process $\gamma \rightarrow e^+ + e^- + \bar{\nu} + \nu$ should also be considered when $\omega_o > 2m$.

In order to integrate numerically equation (A12) by Monte Carlo methods, it is most convenient to transform to a set of variables which range between 0 and 1. We therefore

define $X = (x-\lambda^{-1})/(x_c-\lambda^{-1})$, $Y = (y-\gamma)/(y_c-\gamma)$, $W = (1+w)/2$, and $Z = (1+z)/2$. Here x_c and y_c are arbitrary cutoffs chosen to limit the region of integration of x and y to a finite interval; they are chosen so that the important part of the region of integration is sampled. With these variables, equation (A12) becomes

$$\mathcal{Q} = \frac{m^2(kT)^5}{4(2\pi)^7}\int_0^1 \frac{dX}{(x_c-\lambda^{-1})}\sqrt{x^2-\lambda^{-2}}(e^{x-\nu}+1)^{-1}\int_0^1 \frac{dY}{(y_c-\gamma)}\sqrt{y^2-\gamma^2}(e^{y}-1)^{-1}$$
$$\times\int_0^1 2\,dW\int_0^1 \frac{t^2\,dt}{SD(D+2)}\int_0^1 2\,dZ\,(x+y)\left(1-\frac{S+tGz}{D+2}\right)\left(e^{\nu-\frac{S+tGz}{D+2}(x+y)}+1\right)^{-1} I \qquad (A13).$$

We do the Monte Carlo integration using the method of importance sampling. We define an importance function

$$g(X,Y,Z,W,t) = \mathcal{X}(X)\mathcal{Y}(Y)\mathcal{Z}(Z)\mathcal{W}(W)\mathcal{T}(t),$$

normalized such that

$$\int_0^1\int_0^1\int_0^1\int_0^1\int_0^1 g(X,Y,Z,W,t)dX\,dY\,dZ\,dW\,dt = 1$$

by normalizing $\mathcal{X}$, $\mathcal{Y}$, $\mathcal{Z}$, $\mathcal{W}$, and $\mathcal{T}$ separately. Letting I be the integrand of equation (A13), we actually perform the integral

$$\int \frac{I}{g}g\,dX\,dY\,dZ\,dW\,dt = \int \frac{I}{g}dG_x dG_y dG_z dG_w dG_t \approx \sum_i\left(\frac{I_i}{g_i}\right),$$

where the integration points i are uniformly sampled over the variables $G_x = \int \mathcal{X}dX$, $G_y = \int \mathcal{Y}dY$, etc. A wise choice of g will improve the accuracy of the Monte Carlo integration over the "standard" Monte Carlo integration of equation (A13). We choose the BPS importance function

$$g = Kx^2\sqrt{x^2-\lambda^{-2}}\,y^3\sqrt{y^2-\gamma^2}\,(e^{x-\nu}+1)^{-1}(e^{y}-1)^{-1}\mathcal{T}(t)\mathcal{Z}(z)(e^{\nu-x-x_{av}}+1)^{-1},$$

where K is the normalization constant

$$K = \left(\int_0^1 x^4 \sqrt{x^2 - \lambda^{-2}} (e^{x-\nu} + 1)^{-1} (e^{\nu - x - x_{av}} + 1)^{-1} dX \int_0^1 y^5 \sqrt{y^2 - \gamma^2} (e^y - 1)^{-1} \, dY \right)^{-1},$$

$$\mathcal{T}(t) = 2t,$$

and

$$\mathcal{Z}(z) = 1.$$

The quantity x_{av} is chosen such that $x + x_{av}$ is a typical value of the term $\frac{(S+tGz)(x+y)}{(D+2)}$. BPS uses $x_{av} = 4$, and we do the same.

Table 1

This table presents the coefficients to be used in the fitting formula

$$Q_{approx} = K(\rho,\lambda)e^{-c\xi}\frac{a_0+a_1\xi+a_2\xi^2}{\xi^3+b_1/\lambda+b_2/\lambda^2+b_3/\lambda^3}$$

(see equation 7) which, when summed, gives values within $\approx$20% of the exact numerical values for the total neutrino emissivity in the temperature range $10^{8.2}K \leq T \leq 10^{11}K$.

$10^8K \leq T \leq 10^{10}K$							
	a_0	a_1	a_2	b_1	b_2	b_3	c
pair	5.026×10^{19}	1.745×10^{20}	1.568×10^{21}	9.383×10^{-1}	-4.141×10^{-1}	5.829×10^{-2}	5.5924
photo	3.897×10^{10}	5.906×10^{10}	4.693×10^{10}	6.290×10^{-3}	7.483×10^{-3}	3.061×10^{-4}	1.5654
plasma	2.146×10^{-7}	7.814×10^{-8}	1.653×10^{-8}	2.581×10^{-2}	1.734×10^{-2}	6.990×10^{-4}	0.56457
$10^{10}K < T \leq 10^{11}K$							
pair	5.026×10^{19}	1.745×10^{20}	1.568×10^{21}	1.2383	-8.141×10^{-1}	0.0	4.9924
photo	3.897×10^{10}	5.906×10^{10}	4.693×10^{10}	6.290×10^{-3}	7.483×10^{-3}	3.061×10^{-4}	1.5654
plasma	2.146×10^{-7}	7.814×10^{-8}	1.653×10^{-8}	2.581×10^{-2}	1.734×10^{-2}	6.990×10^{-4}	0.56457

REFERENCES

Acton, Forman S. 1970, *Numerical Methods That Work*, New York: Harper & Row.

Barkat, S. 1975, *Ann. Rev. Astr. and Ap.*, **13**, 45.

Beaudet, G., Petrosian, V. and Salpeter, E. E. 1967, *Ap. J.*, **150**, 979.

Bodenheimer, P. and Woosley, S. E. 1983, *Ap. J.*, **269**, 281.

Chou, C. K., Fassio-Canuto, L. and Canuto, V. 1979, *Ap. J.*, **227**, 974.

Dicus, D. A. 1973, *Phys. Rev. D*, **6**, 941.

Dicus, D. A., Kolb, E. W., Schramm, D. N., and Tubbs, D. L. 1976, *Ap. J.*, **210**, 481.

Flowers, E. 1973, *Ap. J.*, **180**, 911.

Hammersley, J. M. and Handscomb, D. C. 1964, *Monte Carlo Methods*, New York: John Wiley & Sons.

Isern, J., Labay, J., Hernanz, M. and Canal, R. 1983, *Ap. J.*, **273**, 320.

Itoh, N. and Kohyama, Y. 1983, *Ap. J.*, **275**, 858.

Itoh, N., Matsumoto, N., Seki, M. and Kohyama Y. 1984a, *Ap. J.*, **279**, 413.

Itoh, N., Kohyama, Y., Matsumoto, N., and Seki, M. 1984b, *Ap. J.*, **280**, 787.

Itoh, N., Kohyama, Y., Matsumoto, N., and Seki, M. 1984c, *Ap. J.*, **285**, 304.

Joss, P. C. and Li, F. K. 1980, *Ap. J.*, **238**, 287.

Lamb, D. Q. and Van Horn, H. M. 1975, *Ap. J.*, **200**, 306.

Munakata, H., Kohyama, Y., and Itho, N. 1985, *Ap. J.*, **296**, 197.

Nomoto, K. and Tsuruta, S. 1981, *Ap. J. Letters*, **250**, L19.

Ramadurai, S. 1976, *M.N.R.A.S.*, **176**, 9.

Ramadurai, S. 1984, *M.N.R.A.S.*, **206**, 849.

Ray, A., Chitre, S. M., and Kar, K. 1984, *Ap. J.*, **285**, 766.

Soyeur, M. and Brown, G. E. 1979, *Nuc. Phys.*, **A324**, 464.

Sweigart, A. V. and Gross, P. G. 1978, *Ap. J. Supp.*, **36**, 405.

Tayler, R. J. 1981, *Q.J.R.A.S.*, **22**, 93.

FIGURE CAPTIONS

Figure 1: Feynman diagrams for the three neutrino emission mechanisms studied in this paper. The neutral current diagrams are on the left, and the charged current diagrams are on the right. Notice that only electron neutrinos and antineutrinos are produced by the charged current interactions.

Figure 2: The photo, pair, and plasma neutrino emissivities in the Weinberg-Salam theory of the weak interaction with $\sin^2\theta_W = 0.23$ for $T = 10^8$, 10^9, 10^{10}, and $10^{11}K$, respectively. The solid line is the plasma emissivity, the dotted line is the photo emissivity, and the dashed line is the pair emissivity. The pair emissivity is negligible at $T = 10^8K$.

Figure 3: The photo, pair, and plasma neutrino rates for $T = 10^8$, 10^9, 10^{10}, and $10^{11}K$, respectively. The solid line is the plasma rate, the dotted line is the photo rate, and the dashed line is the pair rate. The pair rate is negligible at $T = 10^8K$.

Figure 4: The quantity $E_{av} = \mathcal{Q}/\mathcal{R}$, the average energy of the emitted neutrinos and antineutrinos for $T = 10^8$, 10^9, 10^{10}, and $10^{11}K$, respectively. The solid line is the plasma , the dotted line is the photo , and the dashed line is the pair average energy. The pair rate is negligible at $T = 10^8K$, and so the average energy of neutrinos and antineutrinos emitted by the pair mechanism at 10^8K is not shown.

Figure 5: The quantity $\Delta Q/Q$, where $\Delta Q \equiv (Q - Q_{approx})$, Q is our recalculation of the total neutrino emissivity in the Fermi weak interaction theory, and Q_{approx} is the BPS fitting formula, is plotted as a function of ρ/μ_e for two temperatures, $T = 10^8K$ and $T = 10^{8.1}K$. At 10^8K (a temperature at which BPS numerically calculated the emissivities) the fit is fairly good; the maximum error is $\sim 20\%$. At $10^{8.1}K$, however, the maximum error is $\sim 70\%$.

Figure 6: A comparison of the BPS fitting formula with our Fermi weak interaction theory results for $T = 10^{11} K$. The error is of order 40% over most of the range of density.

Figure 7: A comparison of the BPS fitting formula as modified by Dicus to be correct in the Weinberg-Salam theory with our Weinberg-Salam theory numerical results for three temperatures, $T = 10^{8} K$, $10^{9} K$, and $10^{10} K$.

Figure 8: A comparison of our fitting formula designed to fit the region $10^{10} K < T \leq 10^{11} K$ with our numerical results in that region at two temperatures, $T = 10^{10.5} K$ and $T = 10^{11} K$.

AUTHOR'S ADDRESSES

Paul J. Schinder
Mission Research Corporation
735 State Street
P. O. Drawer 719
Santa Barbara, California 93102

David N. Schramm
Astronomy and Astrophysics Department
The University of Chicago
5640 S. Ellis Avenue
Chicago, Illinois 60637

Paul J. Wiita
Department of Astronomy and Astrophysics E/1
The University of Pennsylvania
Philadelphia, Pennsylvania 19104

Steven H. Margolis
The Aerospace Corp.
P. O. Box 92957
Mail Stop MI-105
Los Angeles, California 90009

David Tubbs
Los Alamos National Laboratory
X-2, MS B220
Los Alamos, New Mexico 87545

Figure 1

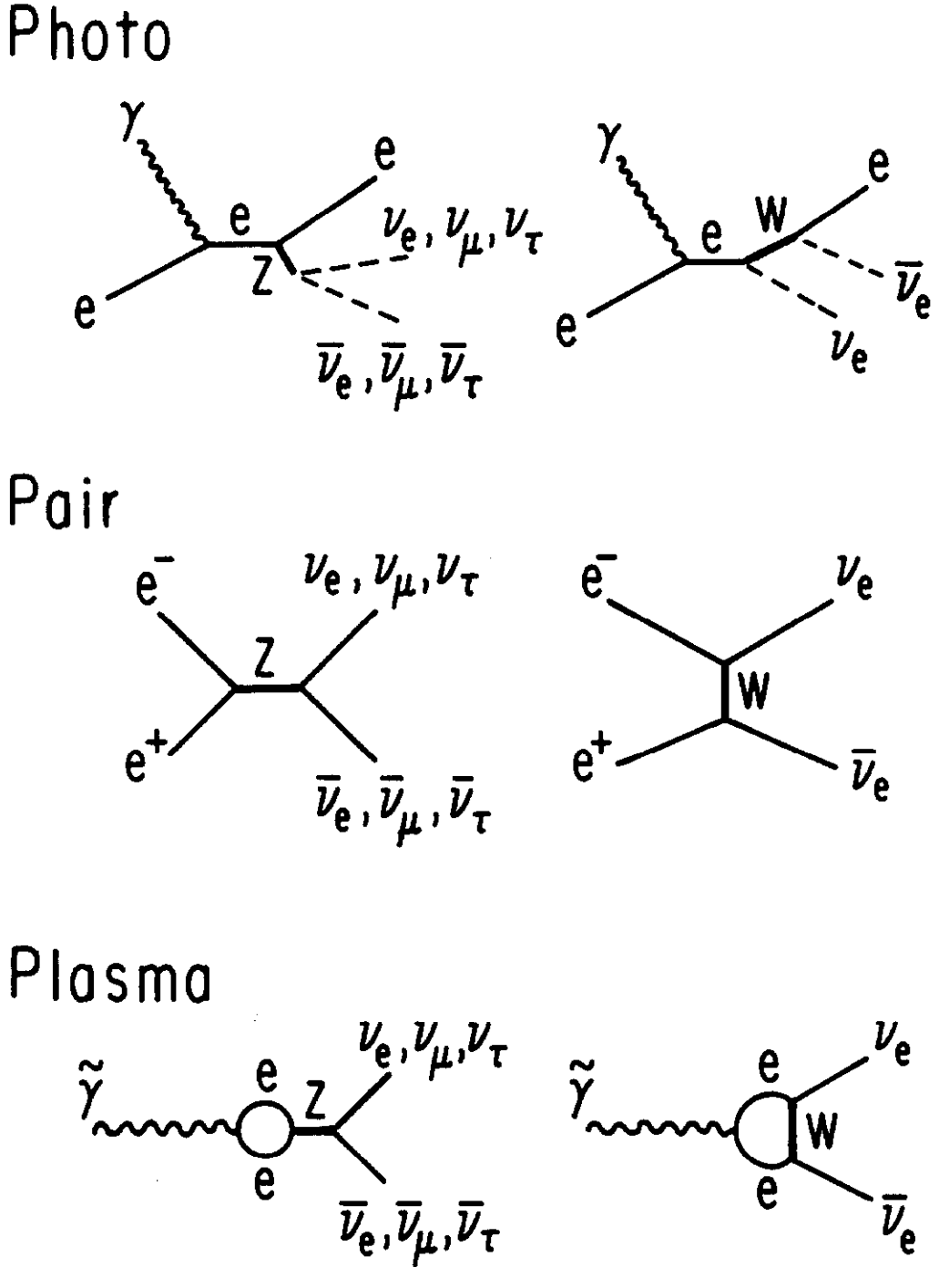
Photo
γ
e
e
Z
ν_e, ν_μ, ν_τ
$\bar{\nu}_e, \bar{\nu}_\mu, \bar{\nu}_\tau$
γ
e
e
W
$\bar{\nu}_e$
ν_e
Pair
e^-
e^+
Z
ν_e, ν_μ, ν_τ
$\bar{\nu}_e, \bar{\nu}_\mu, \bar{\nu}_\tau$
e^-
e^+
W
ν_e
$\bar{\nu}_e$
Plasma
$\tilde{\gamma}$
e
e
Z
ν_e, ν_μ, ν_τ
$\bar{\nu}_e, \bar{\nu}_\mu, \bar{\nu}_\tau$
$\tilde{\gamma}$
e
e
W
ν_e
$\bar{\nu}_e$

Figure 2a

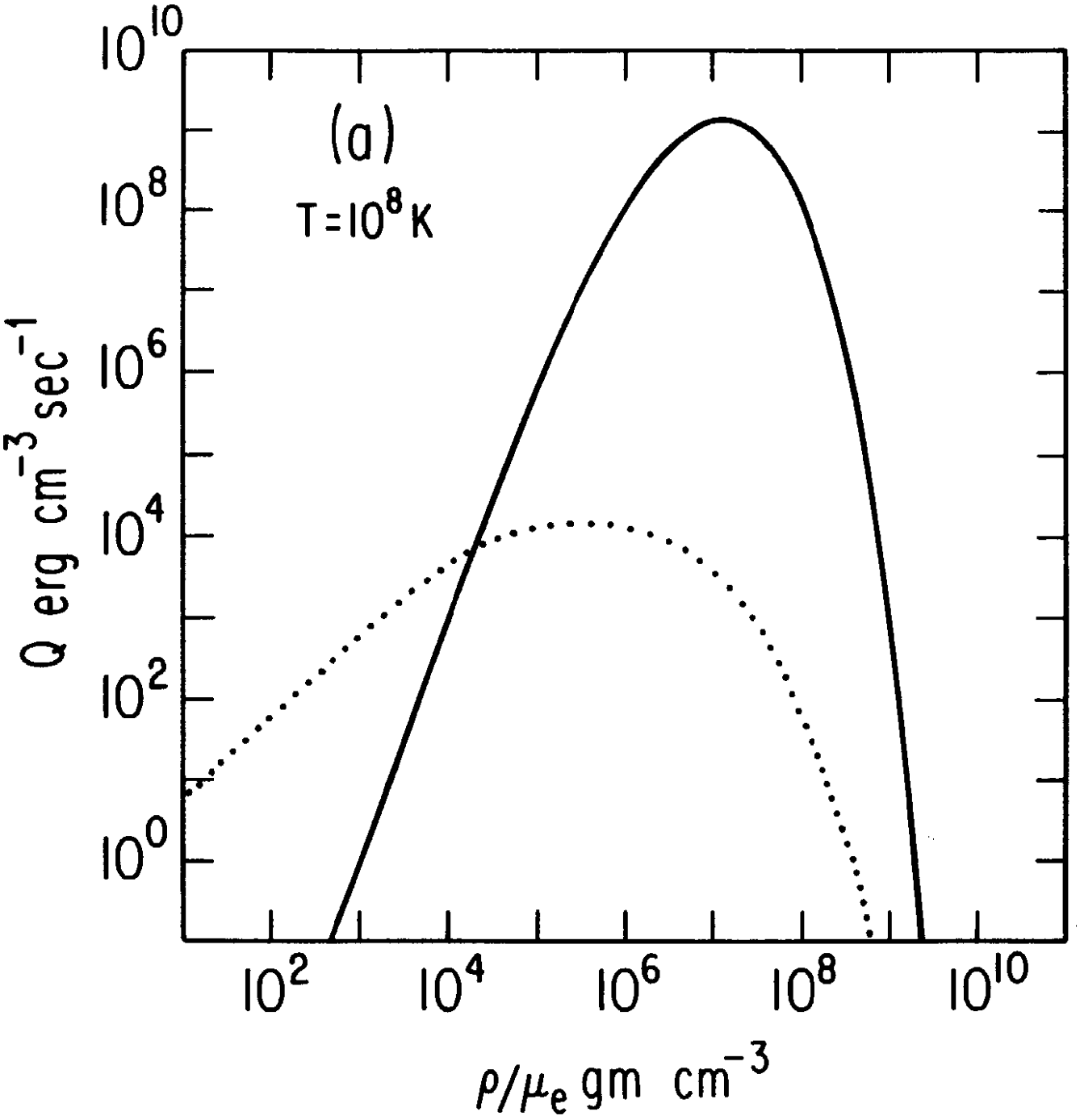

Figure 2b

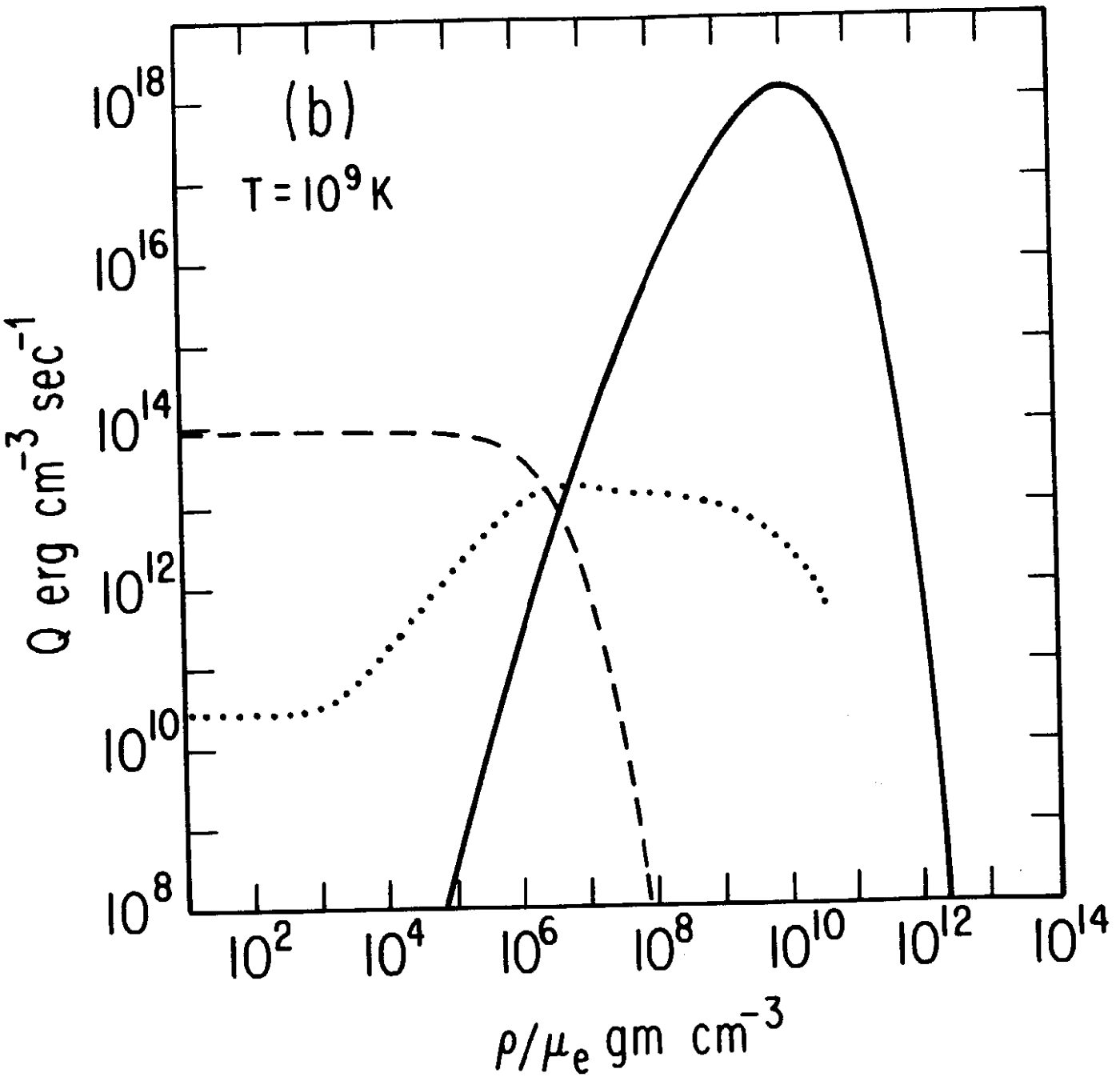
(b)
T = 10^9 K
Q erg cm^-3 sec^-1
10^18
10^16
10^14
10^12
10^10
10^8
10^2
10^4
10^6
10^8
10^10
10^12
10^14
ρ/μ_e gm cm^-3

Figure 2c

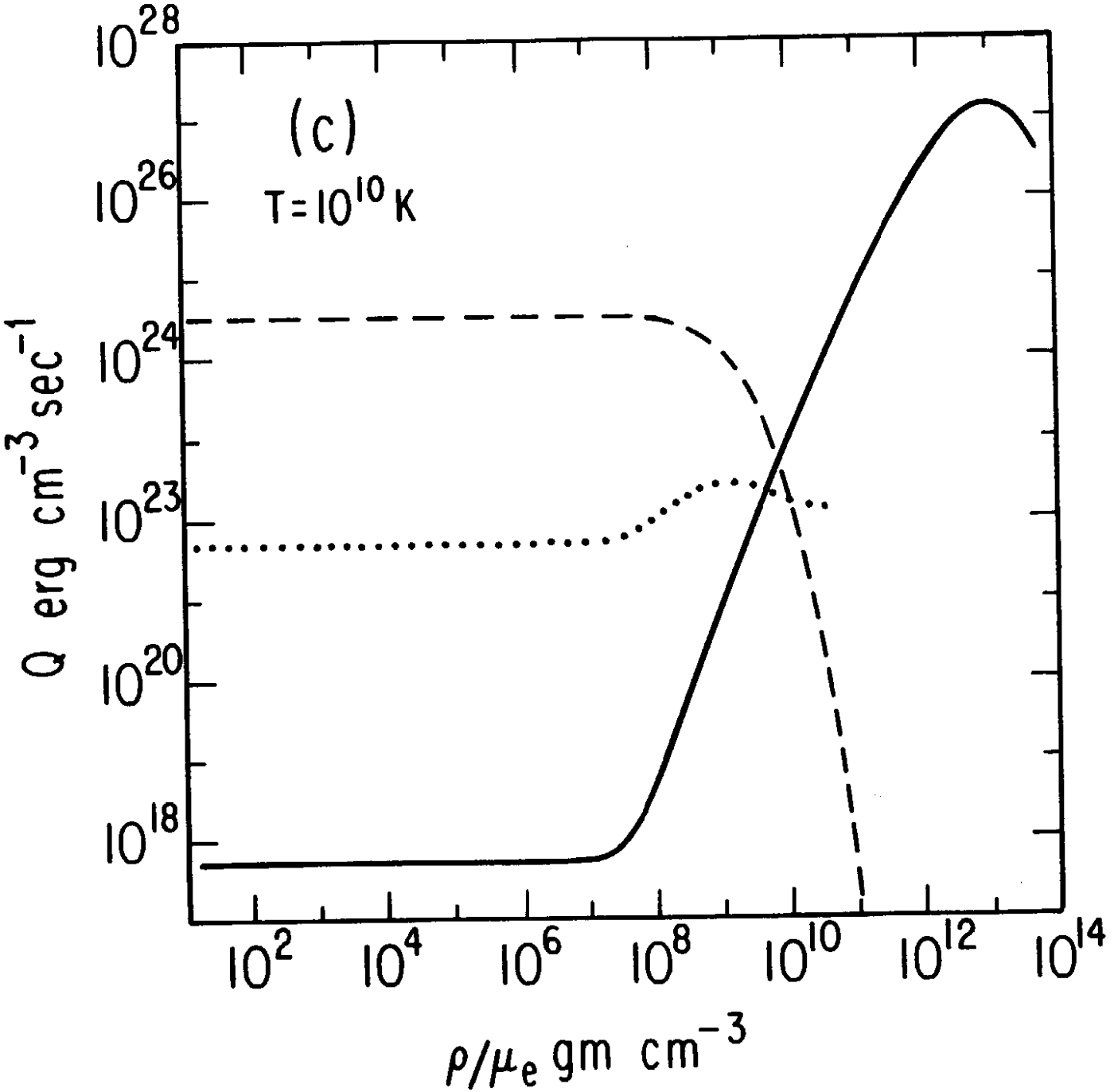
(c)
T=10^10 K
Q erg cm^-3 sec^-1
10^28
10^26
10^24
10^23
10^20
10^18
10^2
10^4
10^6
10^8
10^10
10^12
10^14
ρ/μe gm cm^-3

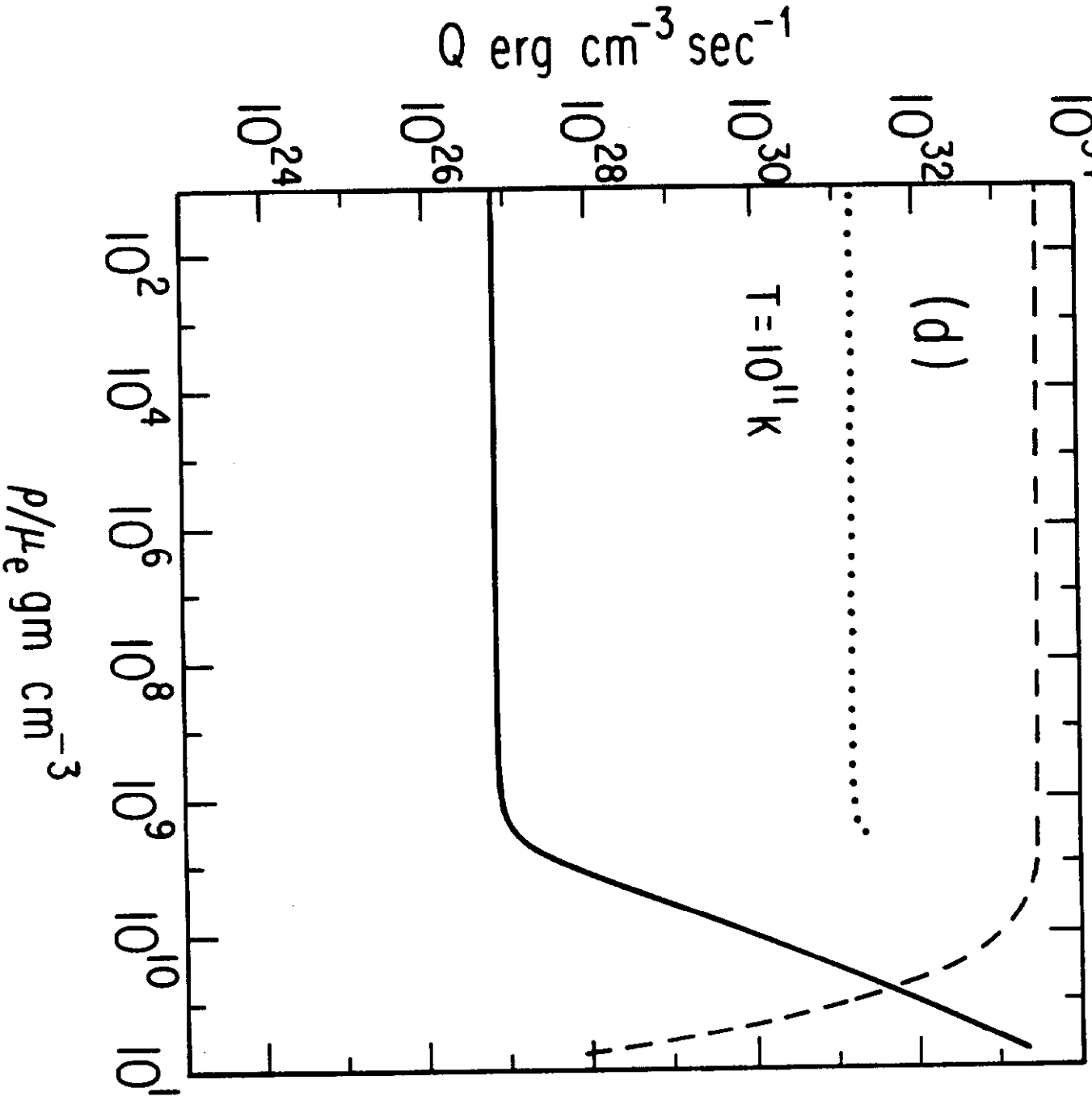
Q erg cm^{-3} sec^{-1}
10^{24}
10^{26}
10^{28}
10^{30}
10^{32}
10^{34}
ρ/μ_e gm cm^{-3}
10^{1}
10^{2}
10^{4}
10^{6}
10^{8}
10^{9}
10^{10}
10^{11}
T=10^{11}K
(d)

Figure 2d

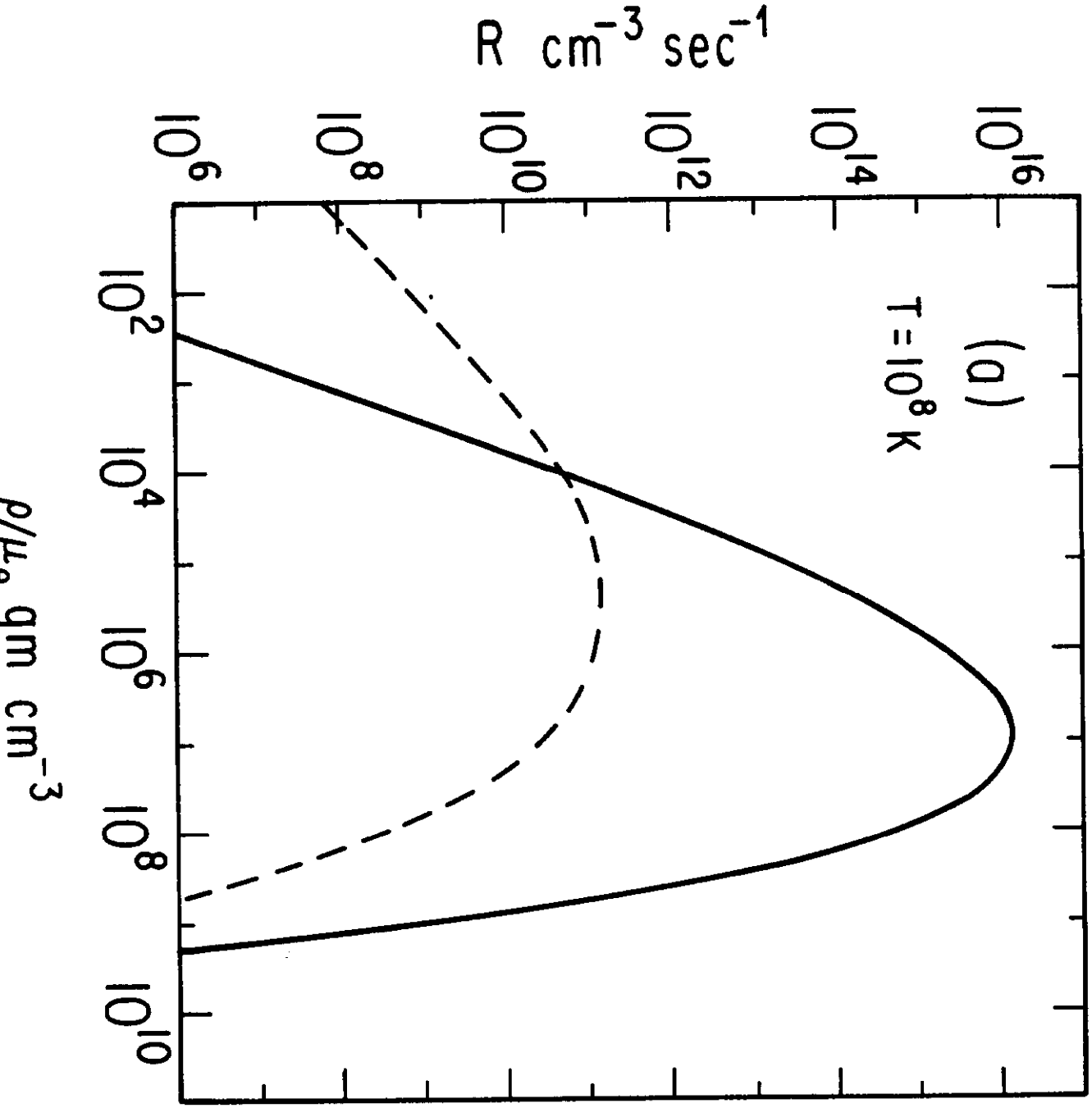
R cm^{-3} sec^{-1}
10^6
10^8
10^{10}
10^{12}
10^{14}
10^{16}
ρ/μ_e gm cm^{-3}
10^2
10^4
10^6
10^8
10^{10}
(a)
T=10^8 K

Figure 3a

Figure 3b

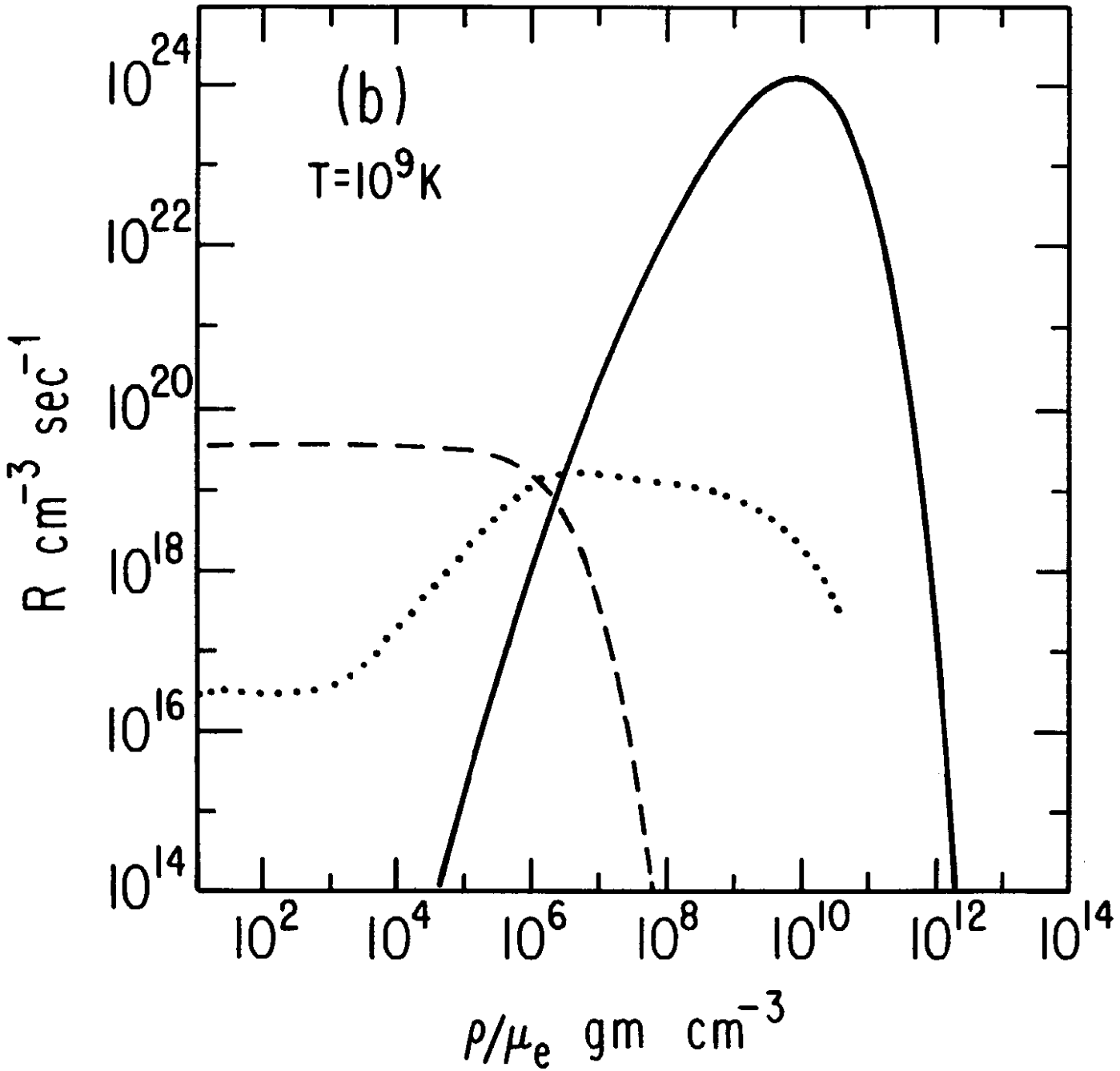
(b)
T=10^9K
R cm^-3 sec^-1
10^24
10^22
10^20
10^18
10^16
10^14
10^2
10^4
10^6
10^8
10^10
10^12
10^14
ρ/μ_e gm cm^-3

Figure 3c

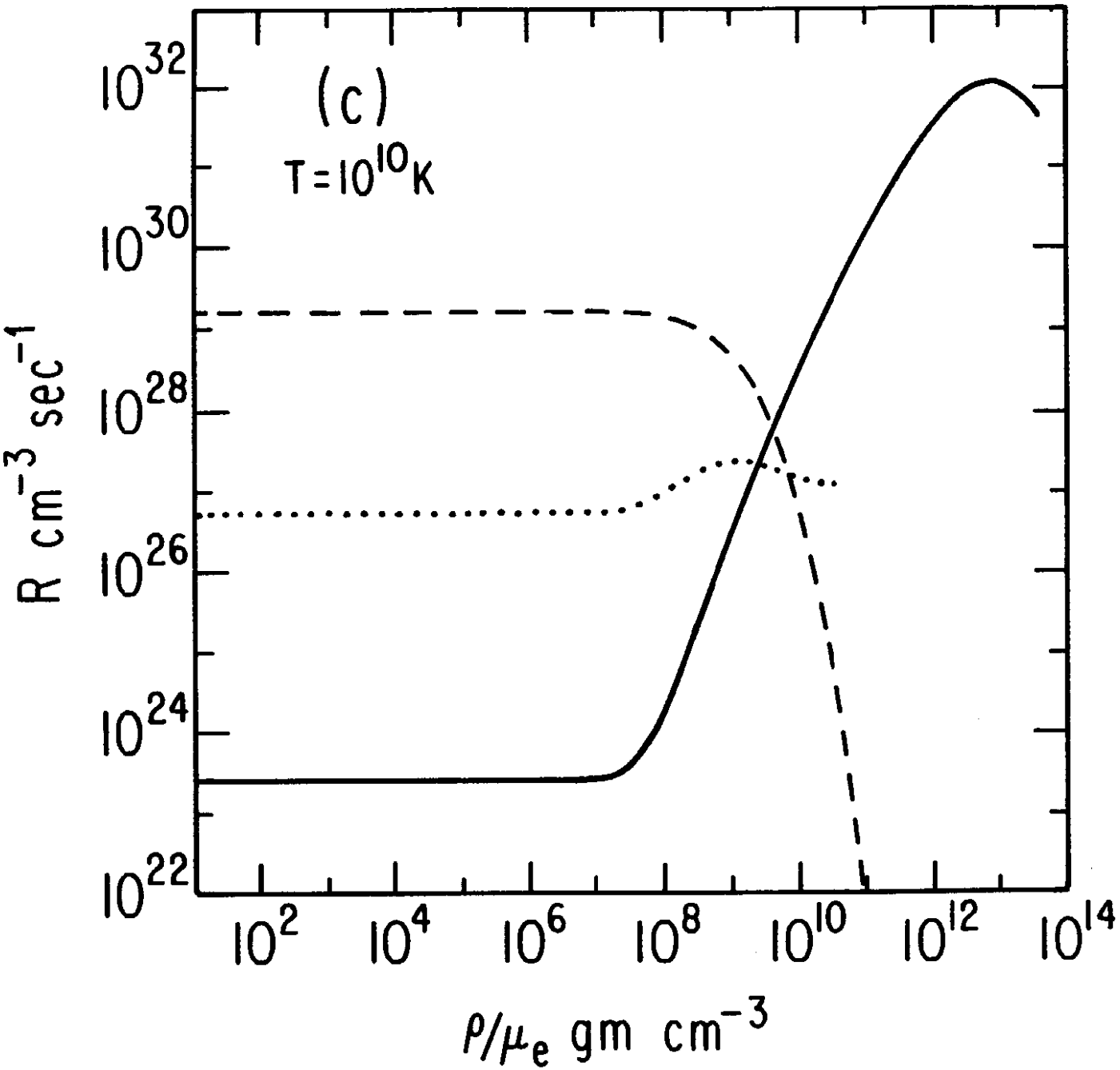
(c)
T=10^10 K
R cm^-3 sec^-1
10^32
10^30
10^28
10^26
10^24
10^22
10^2
10^4
10^6
10^8
10^10
10^12
10^14
ρ/μe gm cm^-3

Figure 3d

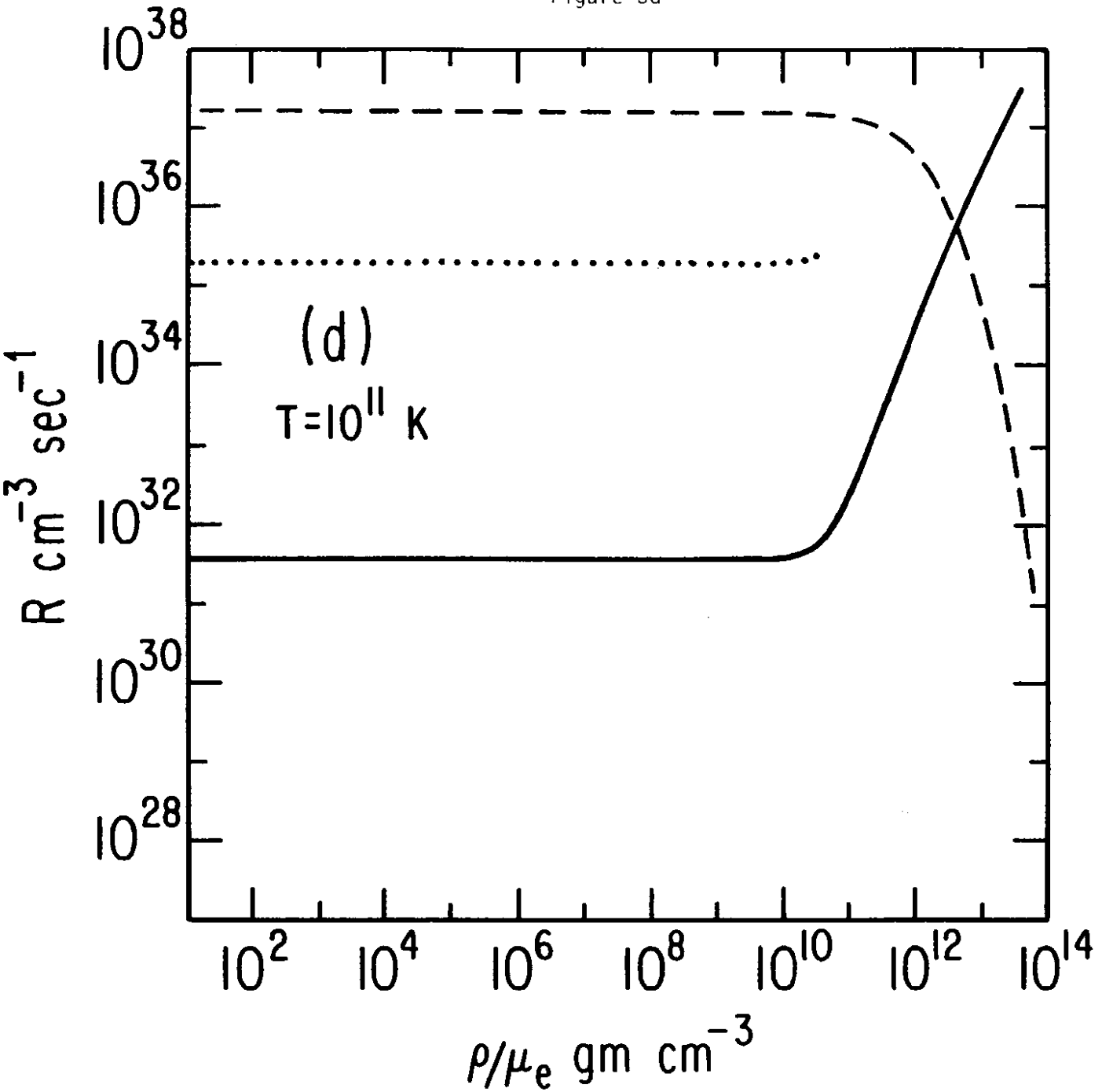
10^{38}
10^{36}
10^{34}
10^{32}
10^{30}
10^{28}
R cm^{-3} sec^{-1}
(d)
T=10^{11} K
10^2 10^4 10^6 10^8 10^{10} 10^{12} 10^{14}
ρ/μ_e gm cm^{-3}

Figure 4a

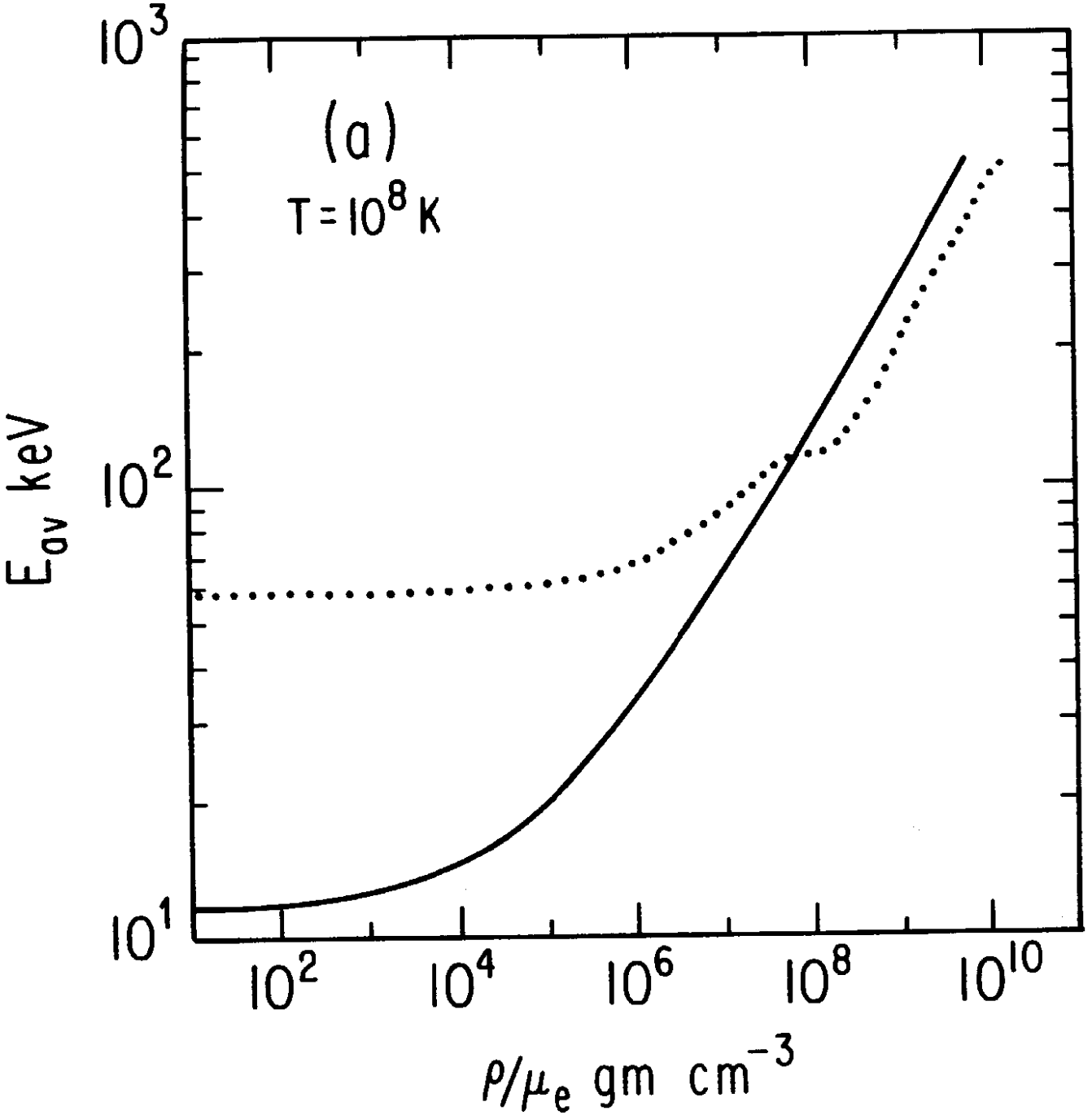

Figure 4b

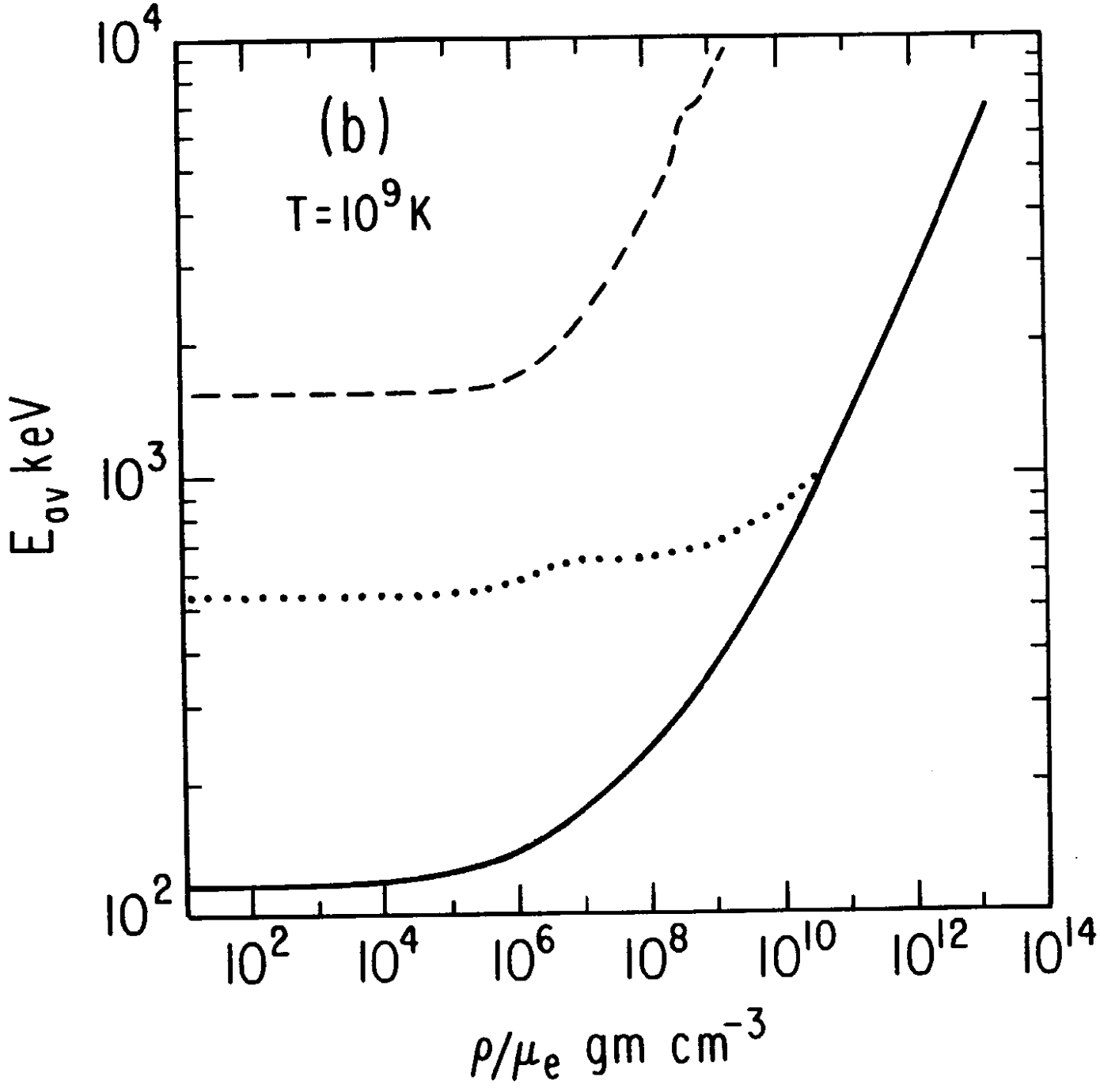
(b)
T=10^9 K
E_ov keV
10^4
10^3
10^2
10^2
10^4
10^6
10^8
10^10
10^12
10^14
ρ/μ_e gm cm^-3

Figure 4c

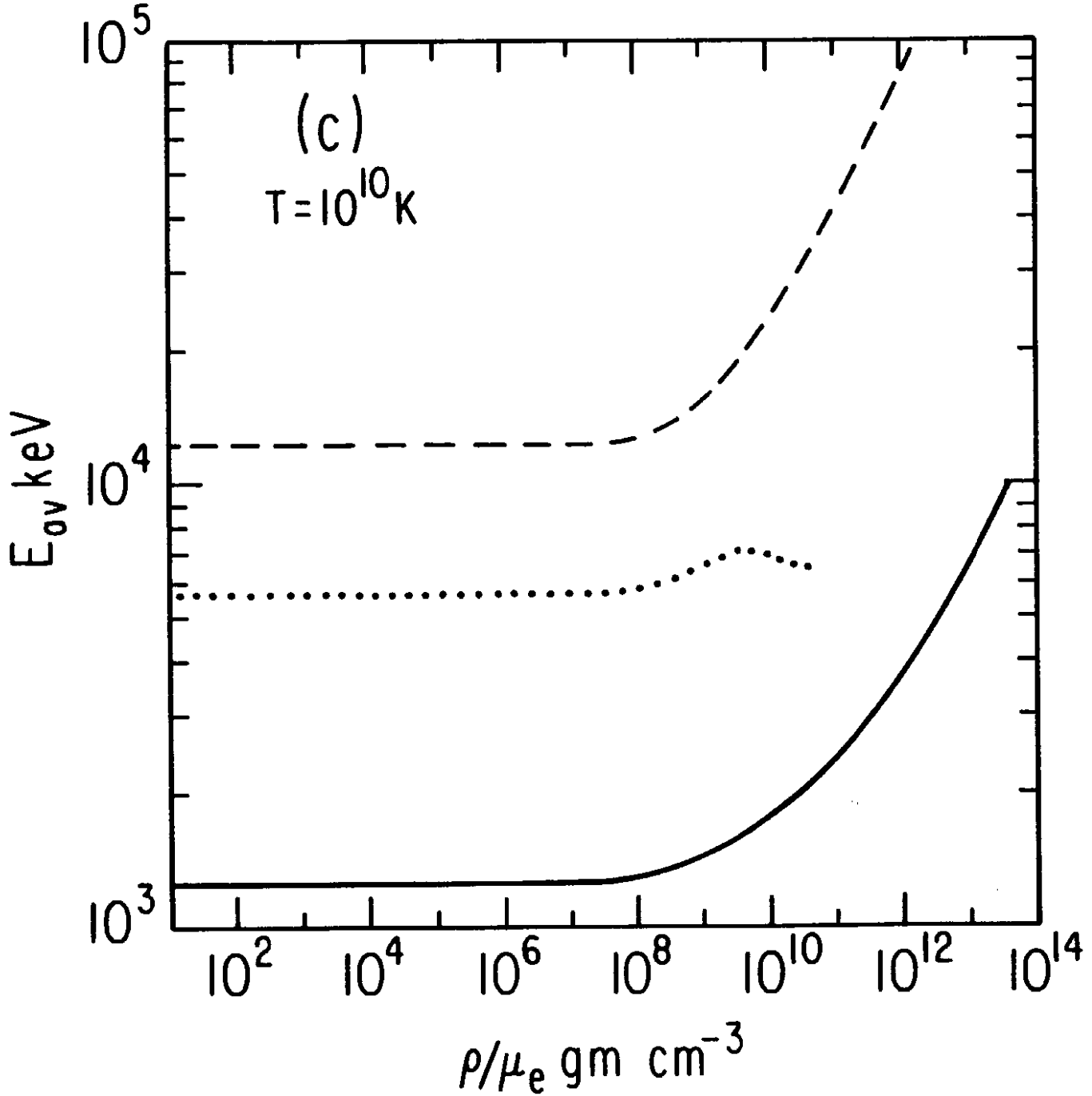
(c)
T=10^10 K
E_ov keV
10^5
10^4
10^3
10^2
10^4
10^6
10^8
10^10
10^12
10^14
ρ/μ_e gm cm^-3

Figure 4d

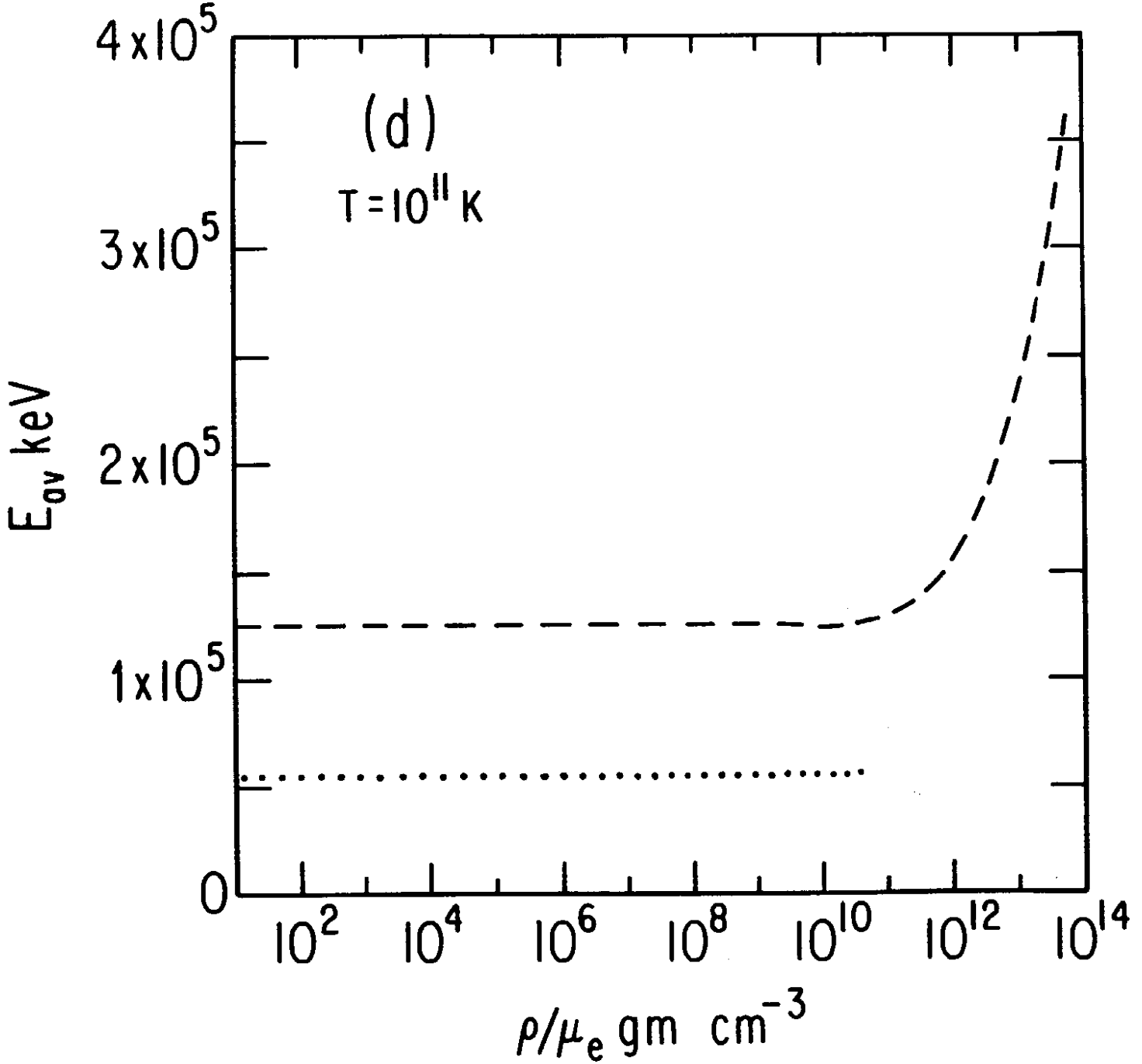
4x10^5
3x10^5
2x10^5
1x10^5
0
(d)
T=10^11 K
E_av keV
10^2
10^4
10^6
10^8
10^10
10^12
10^14
ρ/μ_e gm cm^-3

Figure 5a

Figure 5b

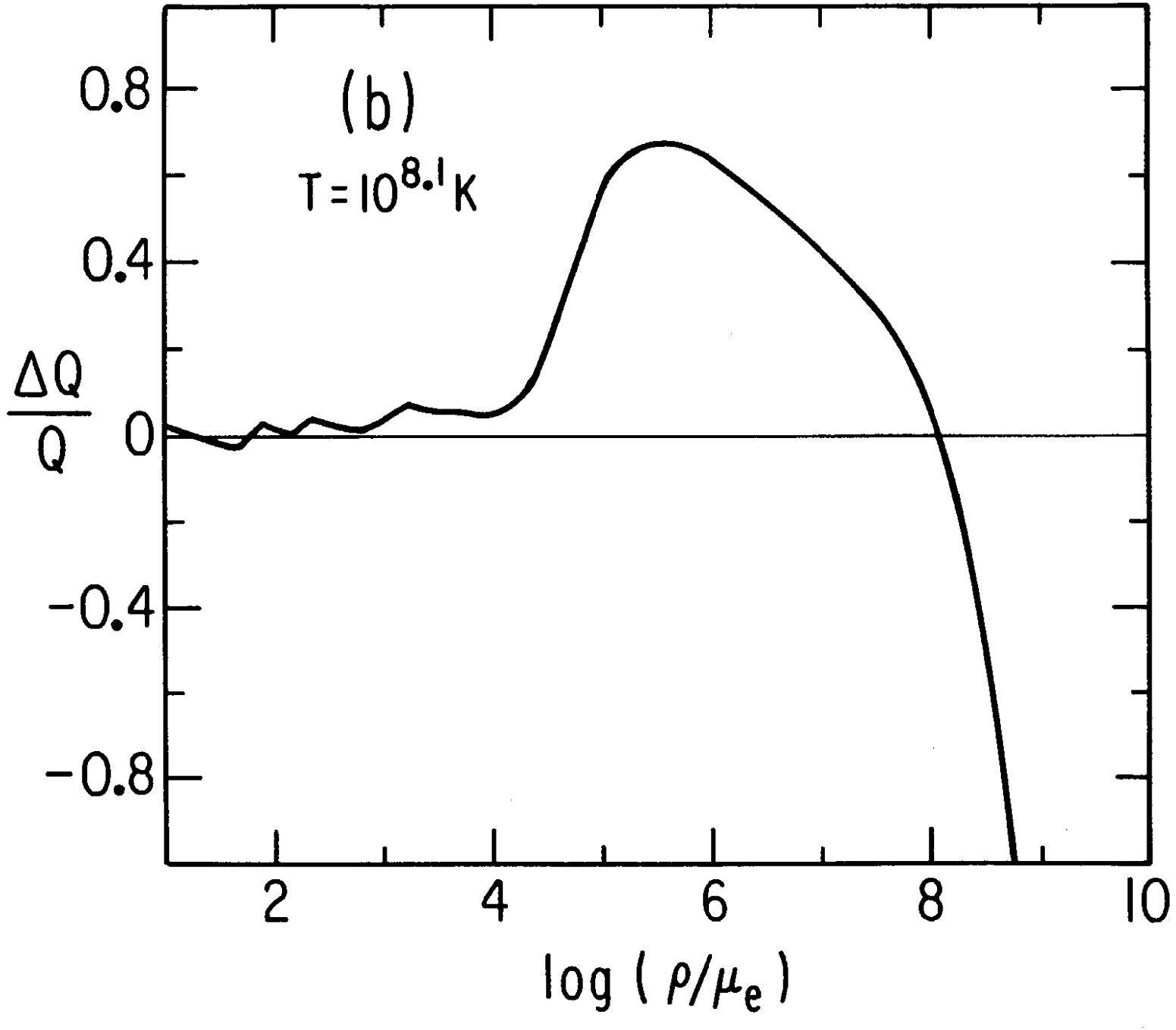

Figure 6

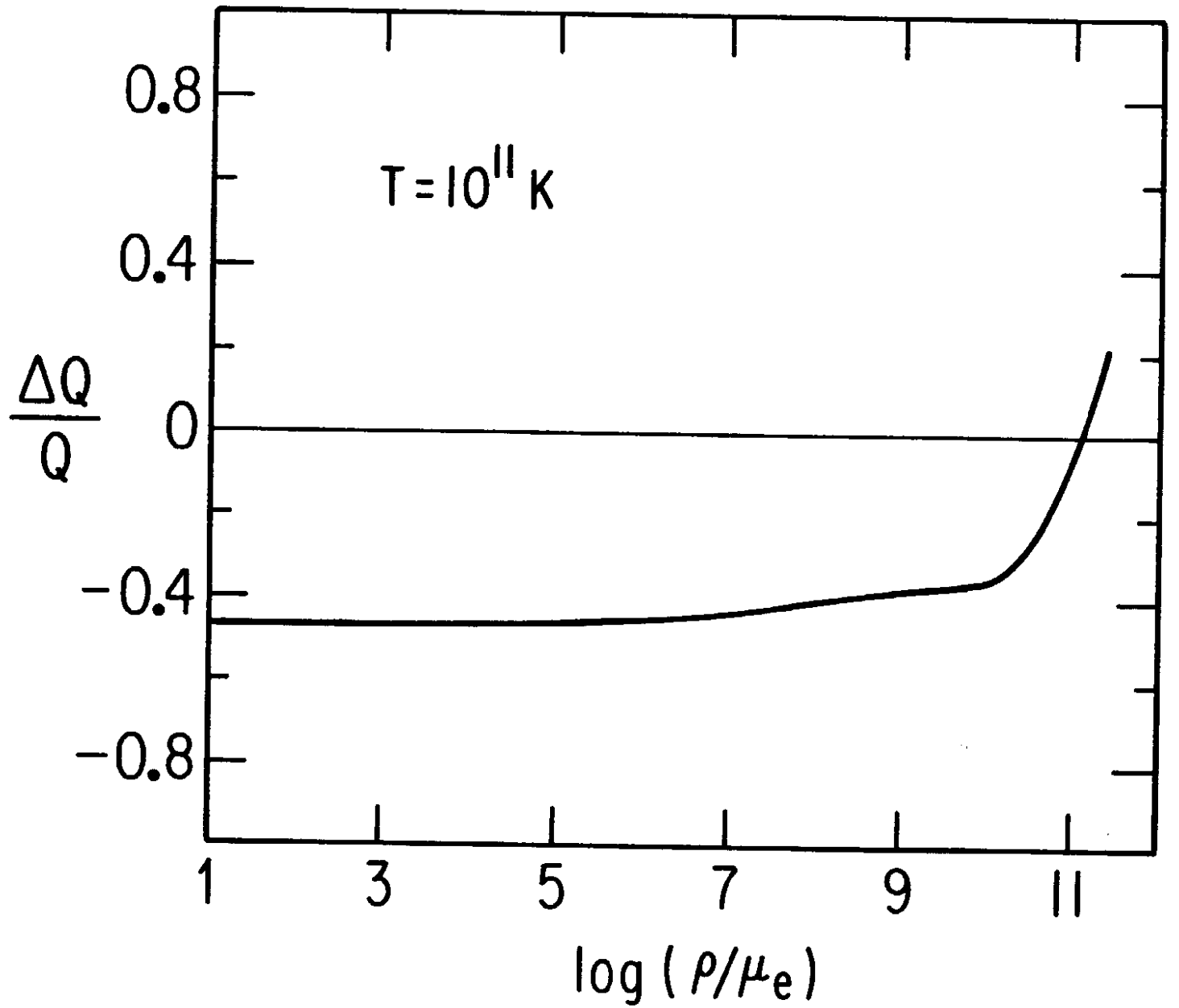

Figure 7a

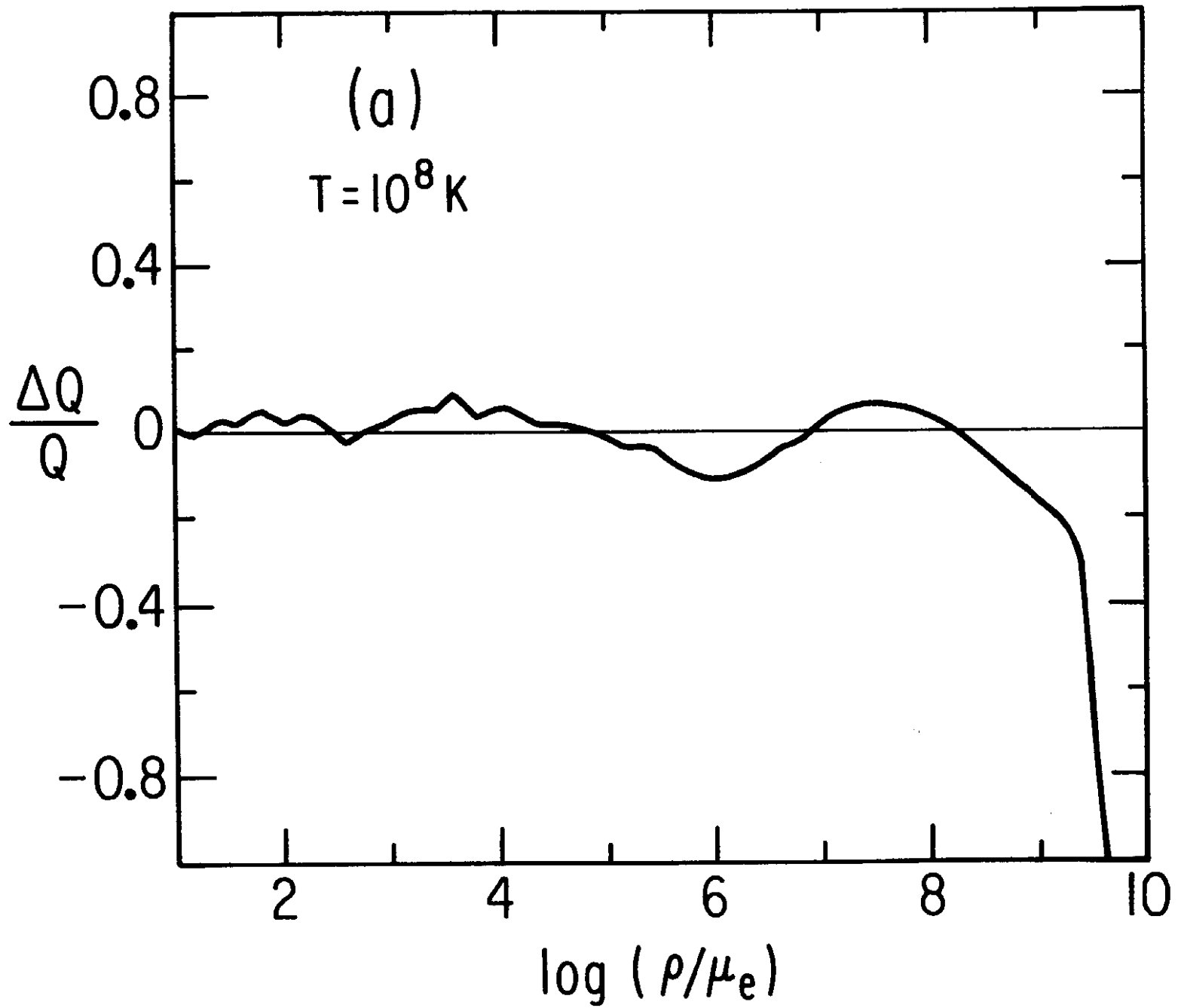

Figure 7b

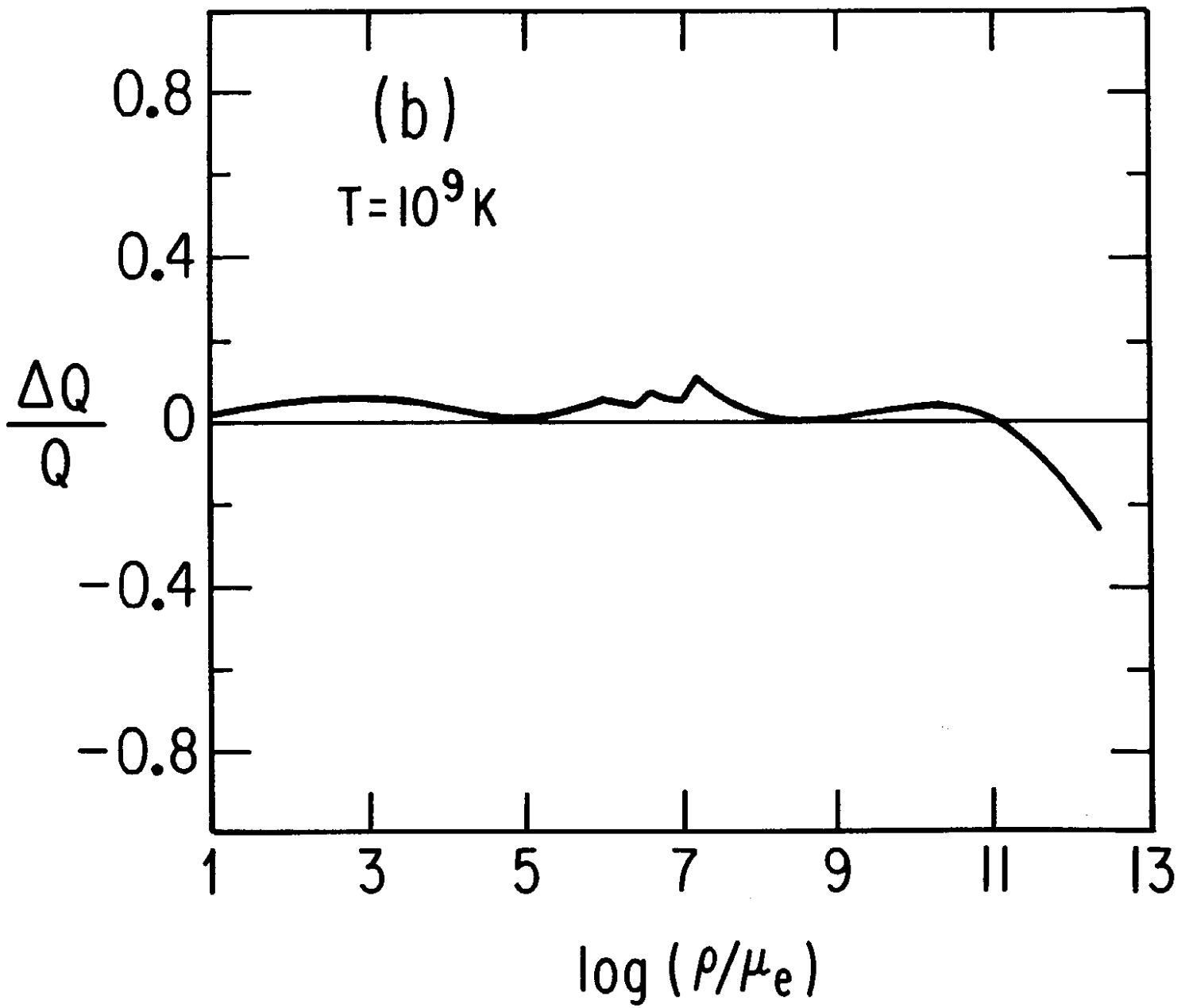

Figure 7c

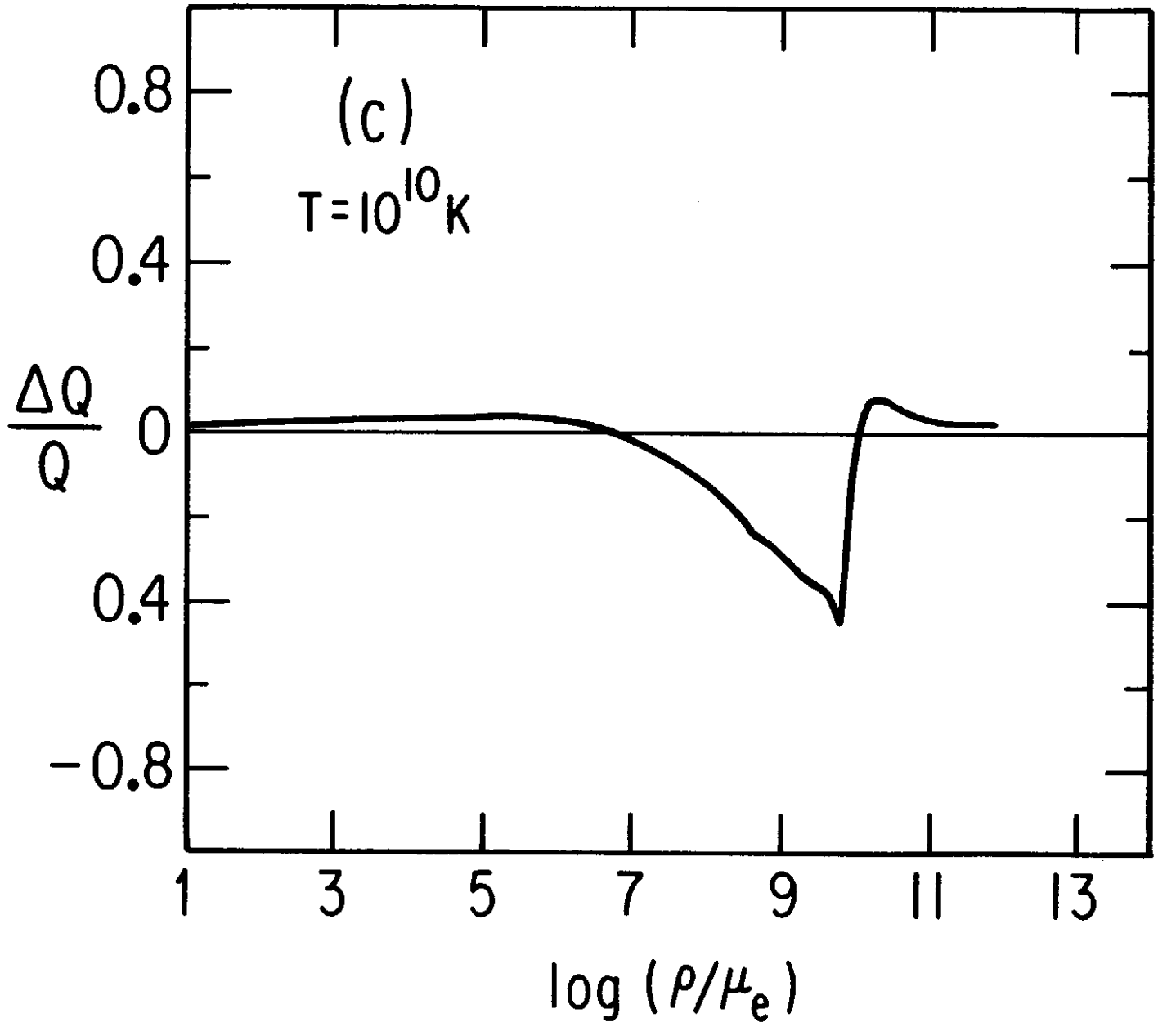

Figure 8a

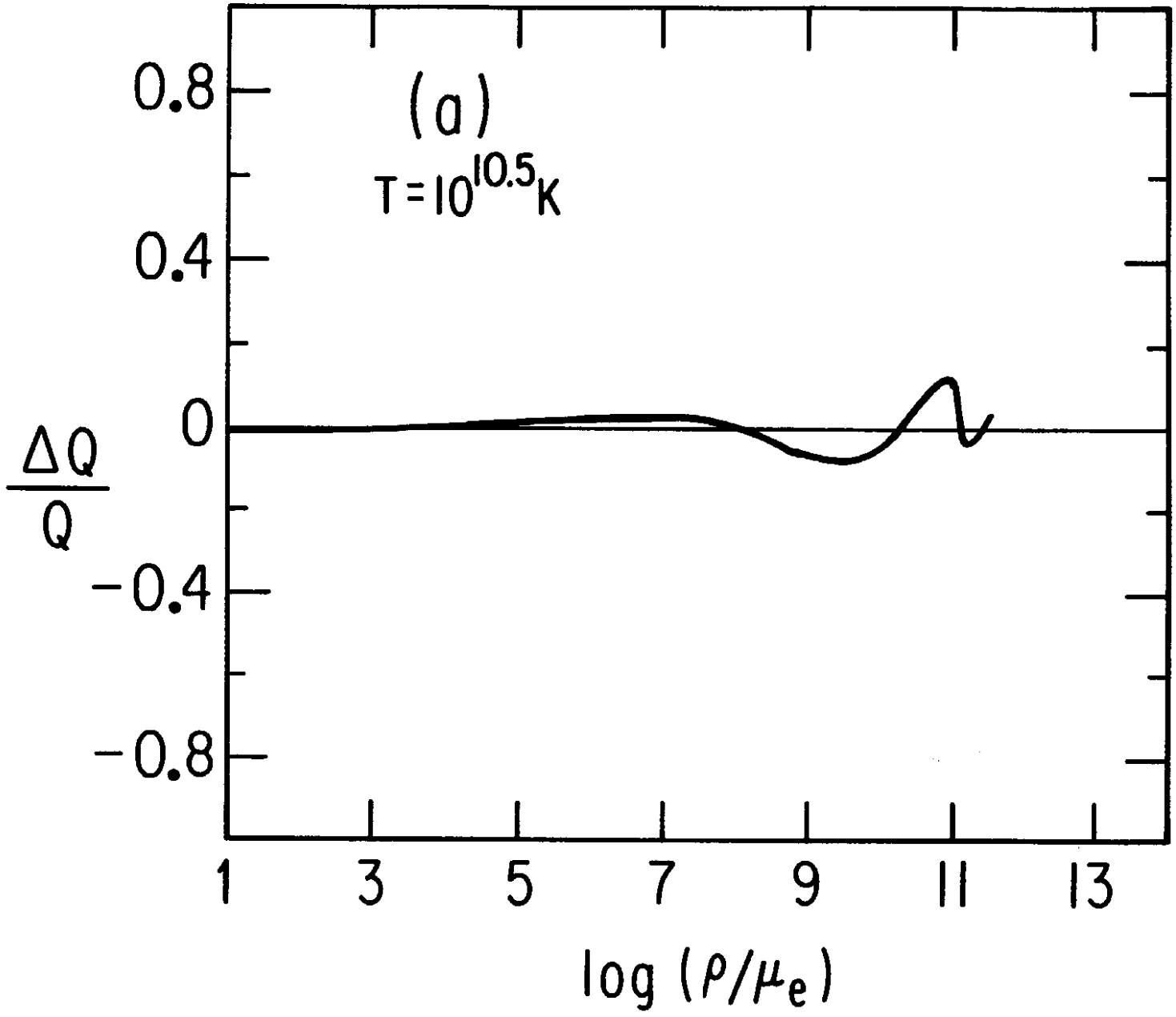

Figure 8b